Eur. Phys. J. C (2017) 77:389
DOI 10.1140/epjc/s10052-017-4943-1

THE EUROPEAN PHYSICAL JOURNAL C

Regular Article - Experimental Physics

Production of $\Sigma(1385)^{\pm}$ and $\Xi(1530)^{0}$ in p–Pb collisions at $\sqrt{s_{\rm NN}} = 5.02$ TeV

ALICE Collaboration[⋆]

CERN, 1211 Geneva 23, Switzerland

Received: 15 February 2017 / Accepted: 24 May 2017

Abstract The transverse momentum distributions of the strange and double-strange hyperon resonances ($\Sigma(1385)^{\pm}$, $\Xi(1530)^{0}$) produced in p–Pb collisions at $\sqrt{s_{\rm NN}} = 5.02$ TeV were measured in the rapidity range $-0.5 < y_{\rm CMS} < 0$ for event classes corresponding to different charged-particle multiplicity densities, $\langle {\rm d}N_{\rm ch}/{\rm d}\eta_{\rm lab}\rangle$. The mean transverse momentum values are presented as a function of $\langle {\rm d}N_{\rm ch}/{\rm d}\eta_{\rm lab}\rangle$, as well as a function of the particle masses and compared with previous results on hyperon production. The integrated yield ratios of excited to ground-state hyperons are constant as a function of $\langle {\rm d}N_{\rm ch}/{\rm d}\eta_{\rm lab}\rangle$. The equivalent ratios to pions exhibit an increase with $\langle {\rm d}N_{\rm ch}/{\rm d}\eta_{\rm lab}\rangle$, depending on their strangeness content.

1 Introduction

Hadrons containing one or more strange quarks have been studied extensively over past decades in connection with the study of quark-gluon plasma [1,2]. Enhanced hyperon yields were observed in heavy-ion collisions with respect to those measured in proton-proton (pp) collisions at the same centre-of-mass energy [3–6]. These enhancements were found to be consistent with those expected from thermal statistical model calculations using a grand canonical ensemble [7]. The canonical [8,9] approach is suggested to explain the relatively suppressed multi-strange baryon yields in smaller collision systems such as pp, proton-nucleus (p–Pb) and peripheral heavy-ion collisions [10].

Short-lived resonances, such as $\rm K^{*0}$ and $\Sigma(1385)^{\pm}$, can be used in heavy-ion collisions to study the hadronic medium between chemical and kinetic freeze-out [11]. Chemical and kinetic freeze-out define the points in time, respectively, when hadron abundances and the momenta of particles stop changing. Decay products of resonances are subject to re-scattering processes and emerge after kinetic decoupling with little memory of the source. Regeneration processes, conversely, increase the resonance yield [12]. If re-scattering processes are dominant over regeneration processes, the measured yield of resonances is expected to be reduced. Moreover, the longer the time between chemical and kinetic freeze-out, the greater the expected reduction.

Recently, the ALICE collaboration reported results on $\rm K^{*0}$, ϕ, Ξ^{-} and Ω^{-} in pp and p–Pb collisions [10,13,14] in addition to Pb–Pb data [6,15]. The evolution of the mean transverse momenta ($\langle p_{\rm T}\rangle$) of mesons and multi-strange baryons were presented as a function of charged-particle multiplicity and particle mass. The observed decrease of the resonance to ground-state ratio $\rm K^{*0}/K^{-}$ has been suggested as an indication of re-scattering processes in the hadronic medium, as first observed in Pb–Pb collisions [15].

This paper reports on the hyperon resonances $\Sigma(1385)^{\pm}$ ($c\tau = 5.48$ fm, uus or dds [16]) and $\Xi(1530)^{0}$ ($c\tau = 22$ fm, uss [16]), measured in p–Pb collisions at $\sqrt{s_{\rm NN}} = 5.02$ TeV. The corresponding results for pp collisions have been previously published in [17]. The results presented in this paper complement the p–Pb results given in [10,14]. The measured $p_{\rm T}$ spectra, yields and mean transverse momenta are presented for different multiplicity classes. Yield ratios of excited to ground-state hyperons are studied as a function of event multiplicity and compared with model predictions [7,18–20]. Considering the similar lifetimes of $\Sigma(1385)^{\pm}$ and $\rm K^{*0}$, a decrease of the $\Sigma(1385)^{\pm}/\Lambda$ ratio, consistent with the decrease observed for the $\rm K^{*0}/K^{-}$ ratio, is expected for increasing system sizes. Hyperon to pion ratios are also presented and compared to the results for ground-state hyperons with the same strangeness contents.

In this paper, the short notations $\Sigma^{*\pm}$ and Ξ^{*0} are adopted for $\Sigma(1385)^{\pm}$ and $\Xi(1530)^{0}$. Moreover, the notations $\Sigma^{*\pm}$ and Ξ^{*0} include the respective anti-particles, namely $\Sigma^{*\pm}$ includes Σ^{*+}, Σ^{*-}, and their anti-particles, while Ξ^{*0} means Ξ^{*0} and $\overline{\Xi^{*}}^{0}$, unless otherwise indicated.

2 Experimental setup and event selection

A description of the ALICE detector and of its performance during the LHC Run 1 (2010–2013) can be found in [21,

⋆ e-mail: alice-publications@cern.ch

Published online: 13 June 2017

Table 1 Mean charged-particle multiplicity densities ($\langle dN_{ch}/d\eta_{lab}\rangle$) measured at midrapidity ($|\eta_{lab}| < 0.5$) [23], corresponding to the multiplicity classes defined using the V0A detector [25] in p–Pb collisions at $\sqrt{s_{NN}} = 5.02$ TeV

V0A percentile (%)	$\langle dN_{ch}/d\eta_{lab}\rangle$
0–20	35.6 ± 0.8
20–40	23.2 ± 0.5
20–60	19.7 ± 0.5
40–60	16.1 ± 0.4
60–100	7.1 ± 0.2
0–100	17.4 ± 0.7

22]. The data sample analysed in this paper was recorded during the LHC p–Pb run at $\sqrt{s_{NN}} = 5.02$ TeV in 2013. Due to the asymmetric energies of the proton (4 TeV) and lead ion (1.57 A TeV) beams, the centre-of-mass system in the nucleon-nucleon frame is shifted in rapidity by $\Delta y_{NN} = 0.465$ towards the direction of the proton beam with respect to the laboratory frame of the ALICE detector [14]. For the analysed p–Pb data set, the direction of the proton beam was towards the ALICE muon spectrometer, the so-called "C" side, standing for negative rapidities; conversely, the Pb beam circulated towards positive rapidities, labelled as "A" side in the following. The analysis in this paper was carried out at midrapidity, in the rapidity window $-0.5 < y_{CMS} < 0$.

The minimum-bias trigger during the p–Pb run was configured to select events by requiring a logical OR of signals in V0A and V0C [22], two arrays of 32 scintillator detectors covering the full azimuthal angle in the pseudorapidity regions $2.8 < \eta_{lab} < 5.1$ and $-3.7 < \eta_{lab} < -1.7$, respectively [23]. In the data analysis it was required to have a coincidence of signals in both V0A and V0C in order to reduce the contamination from single-diffractive and electromagnetic interactions. This left only non-single diffractive (NSD) events, which amount for a total of 100 million events, in the minimum-bias (MB) sample corresponding to an integrated luminosity of about 50 μb^{-1}.

The combined V0A and V0C information discriminates beam-beam interactions from background collisions in the interaction region. Further background suppression was applied in the offline analysis using time information from two neutron zero degree calorimeters (ZDC) [22], as in previous p–Pb analyses [24]. Pile-up events due to more than one collision in the region of beam interaction were excluded by using the silicon pixel detector (SPD) in the inner tracking system (ITS) [22]. The primary vertex (PV) is determined by tracks reconstructed in the ITS and time projection chamber (TPC), and track segments in the SPD [22,23]. MB events are selected when the PV is positioned along the beam axis within ± 10 cm from the centre of the ALICE detector.

The MB events were divided into several multiplicity classes according to the accumulated charge in the forward V0A detector [25]. The $\Sigma^{*\pm}$ resonances are reconstructed in the multiplicity classes 0–20, 20–60, and 60–100%, whereas the Ξ^{*0} analysis is carried out in four classes, namely 0–20, 20–40, 40–60 and 60–100%. To each multiplicity class corresponds a mean charged-particle multiplicity ($\langle dN_{ch}/d\eta_{lab}\rangle$), measured at midrapidity ($|\eta_{lab}| < 0.5$), as shown in Table 1.

3 Data analysis

3.1 Track and topological selections

Table 2 summarizes the relevant information on the measured hyperon resonances, namely the decay modes used in this analysis and their branching ratios. In the case of $\Sigma^{*\pm}$, all states Σ^{*+}, Σ^{*-}, $\overline{\Sigma}^{*-}$ and $\overline{\Sigma}^{*+}$ were separately analysed, while the Ξ^{*0} analysis always includes the charge-conjugated anti-particle, $\overline{\Xi}^{*0}$ due to the limited statistics of the dataset.

In comparison with the $\Sigma^{*\pm}$ and Ξ^{*0} analysis carried out in pp collisions at $\sqrt{s} = 7$ TeV [17], track and topological selections were revised and adapted to the p–Pb dataset; this is notably the case for Ξ^{*0}. Pions from strong decays of both $\Sigma^{*\pm}$ and Ξ^{*0} were selected according to the criteria for primary tracks. As summarized in Table 3, all charged tracks were selected with $p_T > 0.15$ GeV/c and $|\eta_{lab}| < 0.8$, as described in Ref. [22]. The primary tracks were chosen with the distance of closest approach (DCA) to PV of less than 2 cm along the longitudinal direction (DCA_z) and lower than $7\sigma_r$ in the transverse plane (DCA_r), where σ_r is the resolution of DCA_r. The σ_r is strongly p_T-dependent and lower than 100 μm for $p_T > 0.5$ GeV/c [22]. To ensure a good track reconstruction quality, candidate tracks were required to have at least one hit in one of the two innermost layers

Table 2 Properties of the measured resonances and decay modes used in this analysis with total branching ratios [16], obtained as the products of respective branching ratios of daughter particles

	Mass (MeV/c^2)	Width (MeV/c^2)	Decay modes used	Total B.R. (%)
$\Sigma(1385)^+$	1382.80 ± 0.35	36.0 ± 0.7	$\Lambda\pi^+ \to (p\pi^-)\pi^+$	55.6 ± 1.1
$\Sigma(1385)^-$	1387.2 ± 0.5	39.4 ± 2.1	$\Lambda\pi^- \to (p\pi^-)\pi^-$	
$\Xi(1530)^0$	1531.80 ± 0.32	9.1 ± 0.5	$\Xi^-\pi^+ \to (\Lambda\pi^-)\pi^+ \to ((p\pi^-)\pi^-)\pi^+$	42.6 ± 0.3

Table 3 Track selections common to all decay daughters and primary track selections applied to the charged pions from decays of $\Sigma^{*\pm}$ and Ξ^{*0}

Common track selections	$\lvert\eta_{\rm lab}\rvert$	<0.8
	$p_{\rm T}$	>0.15 GeV/c
	PID $\lvert(\mathrm{d}E/\mathrm{d}x)-(\mathrm{d}E/\mathrm{d}x)_{\rm exp}\rvert$	<3 $\sigma_{\rm TPC}$
Primary track selections	DCA$_z$ to PV	<2 cm
	DCA$_r$ to PV	<7 σ_r ($p_{\rm T}$)
	number of SPD points	≥1
	number of TPC points	>70

Table 4 Topological and track selection criteria

	$\Sigma^{*\pm}$	Ξ^{*0}
DCA$_r$ of Λ decay products to PV	>0.05 cm	>0.06 cm
DCA between Λ decay products	<1.6 cm	<1.4 cm
DCA of Λ to PV	<0.3 cm	>0.015 cm
$\cos\theta_\Lambda$	>0.99	>0.875
$r(\Lambda)$	$1.4 < r(\Lambda) < 100$ cm	$0.2 < r(\Lambda) < 100$ cm
$\lvert M_{p\pi} - m_\Lambda\rvert$	<10 MeV/c^2	<7 MeV/c^2
DCA$_r$ of pion (from Ξ^-) to PV		>0.015 cm
DCA between Ξ^- decay products		<1.9 cm
$\cos\theta_\Xi$		>0.981
$r(\Xi^-)$		$0.2 < r(\Xi^-) < 100$ cm
$\lvert M_{\Lambda\pi} - m_\Xi\rvert$		<7 MeV/c^2

(SPD) of the ITS and to have at least 70 reconstructed points in the TPC, out of a maximum of 159. The particle identification (PID) criteria for all decay daughters are based on the requirement that the specific energy loss ($\mathrm{d}E/\mathrm{d}x$) is measured in the TPC within three standard deviations ($\sigma_{\rm TPC}$) from the expected value ($\mathrm{d}E/\mathrm{d}x_{\rm exp}$), computed using a Bethe–Bloch parametrization [22].

Since pions and protons from weak decay of Λ ($c\tau = 7.89$ cm [16]) and pions from weak decay of Ξ^- ($c\tau = 4.91$ cm [16]) are produced away from the PV, specific topological and track selection criteria, as summarized in Table 4, were applied [10,17,26].

In the analysis of $\Sigma^{*\pm}$, secondary π and p from Λ decays were selected with a DCA between the two tracks of less than 1.6 cm and with a DCA$_r$ to the PV greater than 0.05 cm, to remove most primary tracks. For Σ^{*-} and $\overline{\Sigma}^{*+}$, the DCA of Λ to the PV must be smaller than 0.3 cm in order to remove most of the primary weakly-decaying $\Xi(1321)^-$ and $\overline{\Xi}(1321)^+$, which share the same decay channel. The Λ invariant mass ($M_{p\pi}$) was selected within $\pm$ 10 MeV/c^2 of the particle data group (PDG) value ($m_\Lambda = 1115.683 \pm 0.006$ MeV/c^2) [16], the cosine of the pointing angle θ_Λ (the angle between the sum of daughter momenta and the line that connects the PV and the decay vertex, as shown in Fig. 1) was requested to be greater than 0.99, and the radius of the fiducial volume $r(\Lambda)$ (the distance between the PV and the decay vertex) was requested to be between 1.4 and 100 cm.

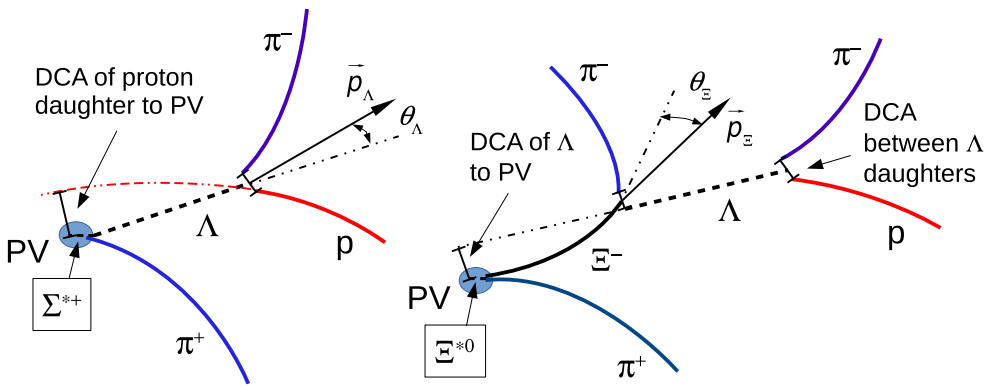

Fig. 1 Sketch of the decay modes for Σ^{*+} (*left*) and Ξ^{*0} (*right*) and depiction of the track and topological selection criteria

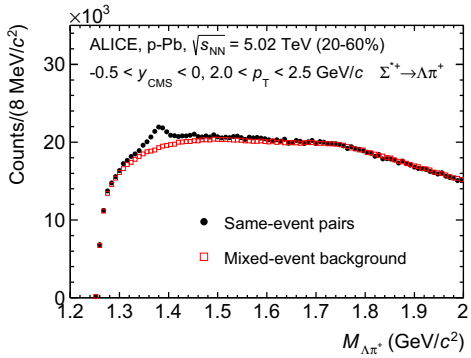

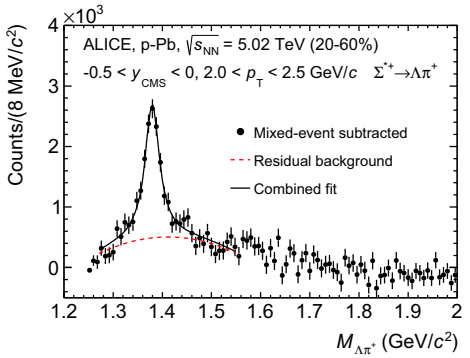

Fig. 2 (*Left*) the $\Lambda\pi^+$ invariant mass distribution (same-event pairs) in $2.0 < p_T < 2.5$ GeV/c and for the multiplicity class 20–60%. The background shape, using pairs from different events (mixed-event background), is normalised to the counts in $1.9 < M_{\Lambda\pi} < 2.0$ GeV/c^2. (*Right*) the invariant mass distribution after subtraction of the mixed-event background. The *solid curve* represents the combined fit, while the *dashed line* describes the residual background

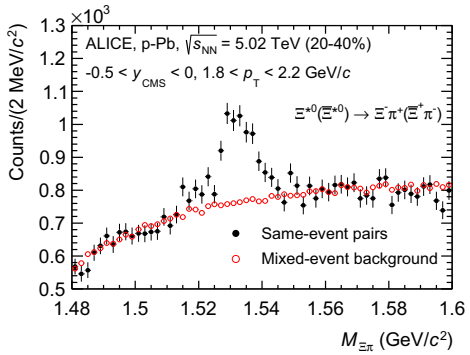

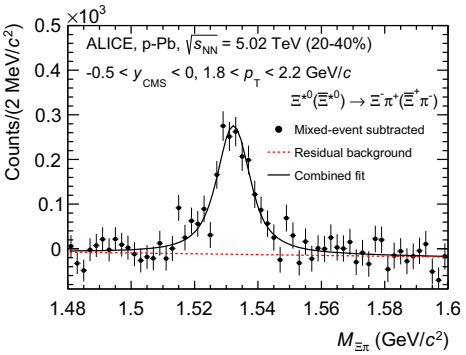

Fig. 3 (*Left*) the $\Xi^\mp\pi^\pm$ invariant mass distribution (same-event pairs) in $1.8 < p_T < 2.2$ GeV/c and for the multiplicity class 20–40%. The background shape, using pairs from different events (mixed-event background), is normalised to the counts in $1.49 < M_{\Xi\pi} < 1.51$ GeV/c^2 and $1.56 < M_{\Xi\pi} < 1.58$ GeV/c^2. (*Right*) the invariant mass distribution after subtraction of the mixed-event background. The *solid curve* represents the combined fit, while the *dashed line* describes the residual background

In the analysis of Ξ^{*0}, Λ and π from Ξ^- were selected with a DCA of less than 1.9 cm and with a DCA$_r$ to the PV greater than 0.015 cm. The Λ daughter particles (π and p) were required to have a DCA$_r$ to the PV greater than 0.06 cm, while the DCA between the two particles was required to be less than 1.4 cm. Cuts on the invariant mass, the cosine of the pointing angle (θ_Λ, θ_Ξ) and the radius of the fiducial volume ($r(\Lambda)$, $r(\Xi)$) in Table 4 were applied to optimize the balance of purity and efficiency of each particle sample.

3.2 Signal extraction

The $\Sigma^{*\pm}$ and Ξ^{*0} signals were reconstructed by invariant-mass analysis of candidates for the decay products in each transverse momentum interval of the resonance particle, and for each multiplicity class. Examples of invariant-mass distributions are presented in the left panels of Figs. 2 and 3 for $\Sigma^{*+}\to\Lambda\pi^+$ and $\Xi^{*0}(\overline{\Xi}^{*0})\to\Xi^-\pi^+(\Xi^+\pi^-)$, respectively.[1]

Since the resonance decay products originate from a position which is indistinguishable from the PV, a significant combinatorial background is present. These background distributions were determined by means of a mixed-event technique, by combining uncorrelated decay products from 5 and 20 different events in the $\Sigma^{*\pm}$ and Ξ^{*0} analyses, respectively. In order to minimise distortions due to different acceptances and to ensure a similar event structure, only tracks from events with similar vertex positions z ($|\Delta z| < 1$ cm) and track multiplicities n ($|\Delta n| < 10$) were taken.

For $\Sigma^{*\pm}$, the mixed-event background distributions were normalised to a p_T-dependent invariant mass region where the mixed-event background and the invariant mass dis-

[1] Similarly to what has been observed in the pp analysis [17], the distributions of Σ^{*-} ($\overline{\Sigma}^{*+}$), not shown in this paper, have an additional peak at ∼1.321 GeV/c^2, as narrow as ∼3 MeV/c^2, due to the residual $\Xi(1321)^-$ ($\overline{\Xi}(1321)^+$), escaping the filter on the DCA of Λ to PV mentioned above.

tribution have similar slopes, as shown in Fig. 2 (left). These p_{T}-dependent invariant mass regions range from $1.5 < M_{\Lambda\pi} < 2.0$ GeV/c^2, for the lowest p_{T} bin, to $1.95 < M_{\Lambda\pi} < 2.0$ GeV/c^2, for the highest p_{T} bin. More details on the normalisation procedure are provided in Ref. [17]. The contribution of the normalisation to the systematic uncertainty was estimated by selecting different normalisation regions and accounts for less than 1%.

For Ξ^{*0}, the mixed-event background distributions were normalised to two fixed regions, $1.49 < M_{\Xi\pi} < 1.51$ GeV/c^2 and $1.56 < M_{\Xi\pi} < 1.58$ GeV/c^2, around the Ξ^{*0} mass peak (Fig. 3 (left)). These regions were used for all p_{T} intervals and multiplicity classes, because the background shape is reasonably well reproduced in these regions and the invariant-mass resolution of the reconstructed peaks appears stable, independently of p_{T}. The uncertainty on the normalisation was estimated by varying the normalisation regions and is included in the quoted systematic uncertainty for the signal extraction (Table 5).

For $\Sigma^{*\pm}$, a combined fit of a second-order polynomial for the residual background description and a Breit–Wigner function with a width fixed to the PDG values [16] for the signal were used in the invariant-mass range of $1.28 < M_{\Lambda\pi} < 1.55$ GeV/c^2. The detector resolution ($\sim$1 MeV/c^2) is much lower than the $\Sigma^{*\pm}$ width and was therefore neglected. In the right panel of Fig. 2, the solid and dashed lines show the result of the combined fit and the residual background, respectively. Alternative fit ranges were taken into account in the estimation of the systematic uncertainty. A linear and a cubic parametrization for the residual background were used to study the systematic uncertainty related to the signal extraction.

For Ξ^{*0}, a combined fit of a first-order polynomial for the residual background and a Voigtian function (a convolution of a Breit–Wigner and a Gaussian function accounting for the detector resolution) for the signal was used, as described in Ref. [17].

The raw yields N^{RAW} were obtained by integrating the signal function from the combined fit. For $\Sigma^{*\pm}$, the integration of the Breit–Wigner function was carried out in the invariant mass range between 1.28 and 1.56 GeV/c^2. For Ξ^{*0}, the integration of the Voigtian function was done in the mass region between 1.48 and 1.59 GeV/c^2. In both cases, corrections for the tails outside the integration region were applied. The statistical uncertainties on the raw yields range between 5 and 15% for $\Sigma^{*\pm}$ and 2–6% for Ξ^{*0}, respectively.

3.3 Corrections and normalisation

The raw yields were corrected for the geometrical acceptance and the reconstruction efficiency (A $\times$ ε) of the detector (Fig. 4) and by branching ratios (total B.R. in Table 2). By using the DPMJET 3.05 event generator [19] and the GEANT 3.21 package [27], a sample of about 100 million p–Pb events was simulated and reconstructed in order to compute the corrections. The distributions of $A \times \varepsilon$ were obtained from the ratio between the number of reconstructed hyperons ($\Sigma^{*\pm}$ or Ξ^{*0}) and the number of generated hyperons in the same p_{T} and rapidity interval. Inefficiencies in the vertex reconstruction have a negligible effect for all multiplicity classes except 60–100%, where a correction factor of 1.03 has to be applied to the raw yields.

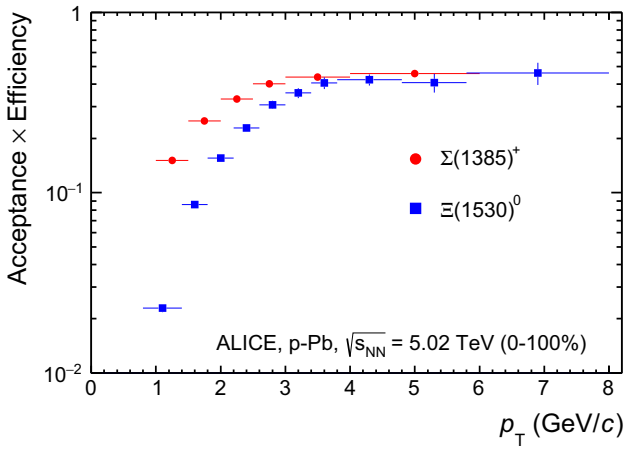

Fig. 4 The geometrical acceptance and the reconstruction efficiency (A $\times$ ε) for Σ^{*+} and Ξ^{*0} in $-0.5 < y_{\mathrm{CMS^{MC}}} < 0$ for minimum-bias events, obtained with DPMJET 3.05 [19] and GEANT 3.1 [27]. Only statistical uncertainties are shown

The product $A \times \epsilon$ for MB events is shown in Fig. 4 for Σ^{*+} and Ξ^{*0}. Since the correction factors for different multiplicity classes are in agreement with those from MB events within statistical uncertainty, the latter were used for all multiplicity classes. For Σ^{*+} and Σ^{*-}, the correction factors were the same. In the case of $\overline{\Sigma}^{*+}$ and $\overline{\Sigma}^{*-}$, correction factors were around 10% higher at low p_{T}, as expected due to the different interaction cross sections of proton and antiprotons in the detector's material [28].

Finally, the yields were normalised to the number of events analysed in each multiplicity class, as defined in Table 1. The MB spectra were instead normalised to the number of NSD events after applying the correction factors for trigger efficiency and event selection, primary vertex reconstruction and selection, resulting in a total scaling factor of 0.964 [14].

3.4 Systematic uncertainties

Systematic effects due to the global tracking efficiency, track and topological selection cuts, PID, mass window selection ($\Xi^{\pm}$), vertex selection, signal extraction and uncertainties on the knowledge of the material budget and branching ratio were studied for each p_{T} interval and multiplicity class by comparing different choices of selection criteria. The results are summarized in Table 5.

Table 5 Summary of the systematic uncertainties on the differential yield, $\mathrm{d}^2N/(\mathrm{d}p_\mathrm{T}\mathrm{d}y)$. Minimum and maximum values in all p_T intervals and multiplicity classes are shown for each source

Source of uncertainty	$\Sigma^{*\pm}$ (%)	Ξ^{*0} (%)
p_T-dependent		
Tracking efficiency	3	3
Tracks selection	1–2	1–2
Topological selection	1–4	1–2
PID	1–3	3–7
Signal extraction	2–5	1–5
Mass window ($\Xi^{\pm}$)	–	4
Vertex selection	1–2	3
p_T-independent		
Material budget	4	4
Branching ratio	1.1	0.3
Total	7–9	8–12

Each source of systematic effects was first requested to pass a consistency check, testing whether a change in selection criteria prevents statistically significant differences in the reconstructed yields [29]. If the source failed the consistency check, the deviation between the default yield and the alternative one obtained by varying the selection was taken as systematic uncertainty. Sources which did not provide statistically significant differences are not listed in Table 5 (e.g. Λ invariant mass window). The uncertainty for the $\Sigma^{*\pm}$ yield is taken as the average of the uncertainties for Σ^{*+}, $\overline{\Sigma}^{*-}$, Σ^{*-}, and $\overline{\Sigma}^{*+}$.

For $\Sigma^{*\pm}$, the main contribution to the total systematic uncertainty originates from the signal extraction, while for Ξ^{*0} the main contribution is from the PID. The signal extraction includes variations of the background normalisation region, choice of the integration interval of the raw yield determination and, in the case of $\Sigma^{*\pm}$, order of the polynomial for describing the residual background. Also, an alternative method, which integrates the signal distribution by summing the bin contents, provides negligible differences.

Table 5 reports the minimum and maximum of the systematic uncertainty from each source. The systematic uncertainty in each p_T interval is obtained as the quadratic sum of all contributions, except the p_T-independent uncertainties, which affect only the normalisation (see Sect. 4.1). The uncertainties which are dependent on multiplicity and uncorrelated across different multiplicity bins were treated separately. Topological selections, signal extraction and PID give the dominant contributions to the uncertainties uncorrelated across multiplicity. These uncertainties were estimated to be within 3% (5%), which represents a fraction of 35% (50%) of the total systematic uncertainty for $\Sigma^{*\pm}$ (Ξ^{*0}).

4 Results and discussion

4.1 Transverse momentum spectra

The transverse momentum spectra of Σ^{*+} and Ξ^{*0} in the rapidity range $-0.5 < y_\mathrm{CMS} < 0$ are shown in Fig. 5 for different multiplicity classes and for NSD events. They cover the ranges $1 < p_\mathrm{T} < 6$ GeV/c for Σ^{*+} and $0.8 < p_\mathrm{T} < 8$ GeV/c for Ξ^{*0}. The spectra obtained for $\overline{\Sigma}^{*-}$, Σ^{*-} and $\overline{\Sigma}^{*+}$ are consistent with the spectrum of Σ^{*+}.

The spectra are fitted with a Lévy–Tsallis function [30],

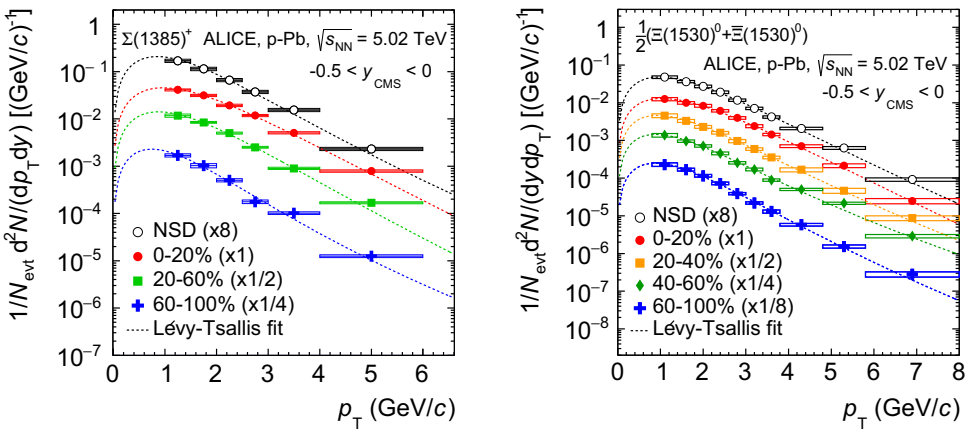

Fig. 5 Transverse momentum spectra of Σ^{*+} (*left*) and Ξ^{*0} (*right*) in different multiplicity classes in the rapidity range $-0.5 < y_\mathrm{CMS} < 0$. For Ξ^{*0}, both particles and antiparticles are analysed together. Statistical (*bars*) and systematic (*boxes*) uncertainties are included. The *dashed curves* are Lévy–Tsallis fit to each individual distribution

Table 6 Integrated yields ($\mathrm{d}N/\mathrm{d}y$) and mean transverse momenta ($\langle p_{\mathrm{T}} \rangle$). The values for $\Sigma^{*\pm}$ are obtained by averaging the values for Σ^{*+}, $\overline{\Sigma}^{*-}$, Σ^{*-} and $\overline{\Sigma}^{*+}$. Statistical (first one) and total systematic (second one) uncertainties including the extrapolation from the various fit functions are quoted

Baryon	Multiplicity class	$\mathrm{d}N/\mathrm{d}y$ ($\times 10^{-3}$)	$\langle p_{\mathrm{T}} \rangle$ (GeV/c)
$\Sigma^{*\pm}$	NSD	$49.0 \pm 0.6 \pm 6.5$	$1.367 \pm 0.009 \pm 0.061$
	0–20%	$90.3 \pm 1.4 \pm 7.9$	$1.495 \pm 0.012 \pm 0.046$
	20–60%	$52.2 \pm 0.8 \pm 6.0$	$1.342 \pm 0.010 \pm 0.055$
	60–100%	$15.2 \pm 0.4 \pm 2.4$	$1.173 \pm 0.015 \pm 0.067$
$1/2(\Xi^{*0} + \overline{\Xi}^{0})$	NSD	$12.5 \pm 0.3 \pm 1.1$	$1.540 \pm 0.016 \pm 0.071$
	0–20%	$27.3 \pm 0.6 \pm 2.8$	$1.626 \pm 0.016 \pm 0.068$
	20–40%	$17.7 \pm 0.5 \pm 2.4$	$1.482 \pm 0.020 \pm 0.100$
	40–60%	$10.7 \pm 0.3 \pm 1.6$	$1.459 \pm 0.025 \pm 0.114$
	60–100%	$3.6 \pm 0.1 \pm 0.5$	$1.377 \pm 0.023 \pm 0.089$

$$\frac{1}{N_{\mathrm{evt}}} \frac{\mathrm{d}^2 N}{\mathrm{d}p_{\mathrm{T}} \mathrm{d}y} = p_{\mathrm{T}} \frac{\mathrm{d}N}{\mathrm{d}y} \frac{(n-1)(n-2)}{nC[nC + m_0(n-2)]} \times \left[1 + \frac{\sqrt{p_{\mathrm{T}}^2 + m_0^2} - m_0}{nC} \right]^{-n}, \quad (1)$$

where N_{evt} is the number of events, m_0 is the mass of the particle, and n, C and the integrated yield $\mathrm{d}N/\mathrm{d}y$ are free parameters for the fit. This function was successfully used to describe most of the identified particle spectra in pp collisions [14,17,26].

The values of $\mathrm{d}N/\mathrm{d}y$ and $\langle p_{\mathrm{T}} \rangle$ shown in Table 6 were calculated by using the experimental spectrum in the measured p_{T}-range and the Lévy–Tsallis fit function outside of the measured p_{T}-range. The contribution from the low-p_{T} extrapolation to the total $\mathrm{d}N/\mathrm{d}y$ is 36–47% (20–29%) for Σ^{*+} (Ξ^{*0}) moving from low to high multiplicity, while the one from the high-p_{T} extrapolation is negligible. The systematic uncertainties on $\mathrm{d}N/\mathrm{d}y$ and $\langle p_{\mathrm{T}} \rangle$ presented in Table 6 were estimated by repeating the Lévy–Tsallis fit moving randomly (with a Gaussian distribution) the measured points within their p_{T}-dependent systematic uncertainties. The p_{T}-independent uncertainties were further added in quadrature to the systematic uncertainties on $\mathrm{d}N/\mathrm{d}y$. Alternative functional forms, such as Boltzmann–Gibbs Blast-Wave [31,32], m_{T}-exponential [32,33], Boltzmann and Bose–Einstein fit functions were used for both particles to evaluate the systematic uncertainties on the low-p_{T} extrapolation. The maximum difference between the results obtained with the various fit functions was taken as the uncertainty. These systematic uncertainties, which vary between 5 and 10%, were added in quadrature to the uncertainties for the Lévy–Tsallis fit. The values for $\Sigma^{*\pm}$ in Table 6 were obtained by averaging those for Σ^{*+}, $\overline{\Sigma}^{*-}$, Σ^{*-} and $\overline{\Sigma}^{*+}$ to reduce the statistical uncertainties.

4.2 Mean transverse momenta

Figure 6 shows the mean transverse momentum $\langle p_{\mathrm{T}} \rangle$ as a function of mean charged-particle multiplicity density $\langle \mathrm{d}N_{\mathrm{ch}}/\mathrm{d}\eta_{\mathrm{lab}} \rangle$ at midrapidity. The results for $\Sigma^{*\pm}$ and Ξ^{*0} are compared with those for other hyperons observed in p–Pb collisions at $\sqrt{s_{\mathrm{NN}}} = 5.02$ TeV [10,24].

Increasing trends from low to high multiplicities are observed for all hyperons. For both $\Sigma^{*\pm}$ and Ξ^{*0}, the mean transverse momenta increase by 20% as the mean charged-particle multiplicity increases from 7.1 to 35.6. This result is similar to the one obtained for the other hyperons. Furthermore, a similar increase has been observed also for $\mathrm{K}^{\pm}$, $\mathrm{K}^0_{\mathrm{S}}$, $\mathrm{K}^*(892)^0$ and ϕ [14], whereas protons are subject to a larger ($\sim$33%) increase in the given multiplicity range, as discussed also in Ref. [24].

In all multiplicity classes, the $\langle p_{\mathrm{T}} \rangle$ follows an approximate mass ordering: $\langle p_{\mathrm{T}} \rangle_{\Lambda} < \langle p_{\mathrm{T}} \rangle_{\Xi^-} \simeq \langle p_{\mathrm{T}} \rangle_{\Sigma^{*\pm}} < \langle p_{\mathrm{T}} \rangle_{\Xi^{*0}} < \langle p_{\mathrm{T}} \rangle_{\Omega^-}$. The $\langle p_{\mathrm{T}} \rangle$ of $\Sigma^{*\pm}$ looks systemati-

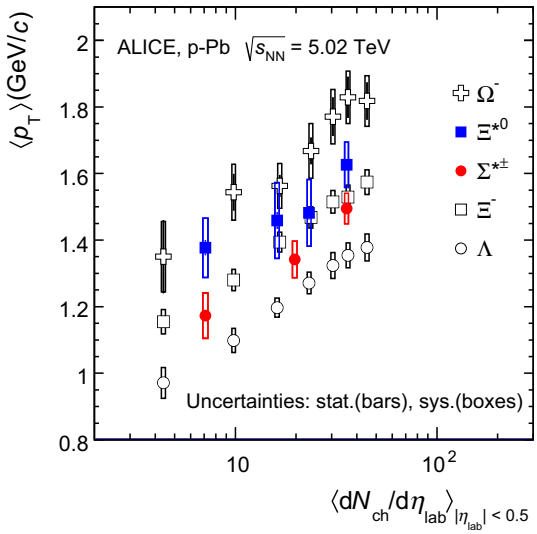

Fig. 6 Mean transverse momenta $\langle p_{\mathrm{T}} \rangle$ of Λ, Ξ^-, $\Sigma^{*\pm}$, Ξ^{*0} and Ω^- in p–Pb collisions at $\sqrt{s_{\mathrm{NN}}} = 5.02$ TeV as a function of mean charged-particle multiplicity density $\langle \mathrm{d}N_{\mathrm{ch}}/\mathrm{d}\eta_{\mathrm{lab}} \rangle$, measured in the pseudorapidity range $|\eta_{\mathrm{lab}}| < 0.5$. The results for Λ, Ξ^- and Ω^- are taken from [10,14,24]. Statistical and systematic uncertainties are represented as *bars* and *boxes*, respectively. The Ω^- and Ξ^- points in the 3rd and 4th lowest multiplicity bins are slightly displaced along the abscissa to avoid superposition with the Ξ^{*0} points

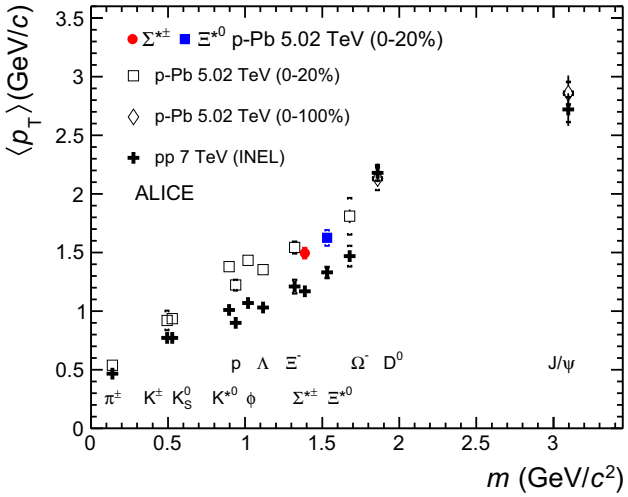

Fig. 7 Mass dependence of the mean transverse momenta of identified particles for the 0–20% V0A multiplicity class and with $-0.5 < y_{\rm CMS} < 0$ in p–Pb collisions at $\sqrt{s_{\rm NN}} = 5.02$ TeV [10,24], and in minimum-bias pp collisions at $\sqrt{s} = 7$ TeV [17] with $|y_{\rm CMS}| < 0.5$. Additionally, D^0 and J/ψ results are plotted. The D^0 and J/ψ were measured in different rapidity ranges: $|y_{\rm CMS}| < 0.5$ [34] ($|y_{\rm CMS}| < 0.9$ [35]) for D^0 (J/ψ) in pp and $-0.96 < y_{\rm CMS} < 0.04$ [34] ($-1.37 < y_{\rm CMS} < 0.43$ [36]) for D^0 (J/ψ) in p–Pb. Note also that the results for D^0 and J/ψ in p–Pb collisions are for the 0–100% multiplicity class

cally lower than the $\langle p_{\rm T} \rangle$ of Ξ^-, despite the larger mass of $\Sigma^{*\pm}$. The uncertainties, however, are too large to draw any conclusion on possible hints of violation of the mass hierarchy. This hierarchy of mass-ordering, also including D^0 and J/ψ in the comparison, is displayed in Fig. 7. Note, however, that the D^0 and J/ψ were measured in different rapidity ranges: $|y_{\rm CMS}| < 0.5$ [34] ($|y_{\rm CMS}| < 0.9$ [35]) for D^0 (J/ψ) in pp and $-0.96 < y_{\rm CMS} < 0.04$ [34] ($-1.37 < y_{\rm CMS} < 0.43$ [36]) for D^0 (J/ψ) in p–Pb, and the results for D^0 and J/ψ in p-Pb collisions are for the 0–100% multiplicity class. This mass dependence is observed in both p–Pb and pp collisions. It was observed also by the STAR collaboration [37] in MB pp, MB d–Au and central Au–Au collisions.

Furthermore, for the light-flavour hadrons, the mean transverse momenta in p–Pb collisions are observed to be consistently higher than those in pp collisions at 7 TeV. The situation for the charm hadrons is different, where $\langle p_{\rm T} \rangle$ appears compatible between both colliding systems. The discrepancy is likely due to different production mechanisms for heavy and light flavours and to a harder fragmentation of charm quarks. Specifically, the fact that $\langle p_{\rm T} \rangle$ remains similar in pp and in p–Pb is consistent with (i) the fact that p–Pb collisions can be considered as a superposition of independent nucleon-nucleon collisions for what concerns D-meson production, as described in [34], and/or (ii) with the effects of shadowing in p–Pb which reduces the production at low $p_{\rm T}$ and thus increasing the overall $\langle p_{\rm T} \rangle$ for J/ψ [36]; the small $p_{\rm T}$ hardening expected in pp when going from 5.02 to 7 TeV is apparently not enough to counter-balance the situation.

Because of small decrease of the $\langle p_{\rm T} \rangle$ for proton and Λ relative to those for $\rm K^{*0}$ and ϕ, two different trends for mesons and baryons have been suggested [38]. Even including D^0 and J/ψ, as shown in Fig. 7, a different trend for mesons and baryons cannot be convincingly established.

4.3 Integrated particle ratios

The integrated yield ratios of excited to ground-state hyperons [10,17,24,32,37,39] with the same strangeness content, for different collision systems and energies, are shown in Fig. 8 as a function of $\langle {\rm d}N_{\rm ch}/{\rm d}\eta_{\rm lab} \rangle$. In both cases, the variation of the integrated yield ratio with mean multiplicity is within experimental uncertainties. In fact, the similar flat behaviour of $\Sigma^{*\pm}/\Lambda$ and Ξ^{*0}/Ξ^- is remarkable, when considering their different lifetimes and other properties such as spin and mass.

The results are compared with model predictions, PYTHIA8 for pp at 7 TeV [20] and DPMJET for p–Pb at 5.02 TeV [19] collisions. The $\Sigma^{*\pm}/\Lambda$ ratios are consistent with the values predicted by PYTHIA8 in pp collisions, whereas the DPMJET prediction for p–Pb collisions is lower than the experimental data. The measured Ξ^{*0}/Ξ^- ratios appear higher than the corresponding predictions for both systems. Note that the PYTHIA8 [20] and DPMJET [19] values in Figs. 8 and 9 were obtained respectively for INEL pp and NSD p–Pb events, which have corresponding mean charged-particle multiplicities of $\langle {\rm d}N_{\rm ch}/{\rm d}\eta_{\rm lab} \rangle_{\rm INEL} = 4.60\ ^{+0.34}_{-0.17}$ [40] and $\langle {\rm d}N_{\rm ch}/{\rm d}\eta_{\rm lab} \rangle_{\rm NSD} = 17.4 \pm 0.7$ [23]. These predictions are indicated as dotted and dashed lines with arbitrary lengths in the pertinent multiplicity regions in Figs. 8 and 9. Fig. 9 will be discussed later.

The results are also compared to thermal model predictions [7,18]. For small systems a canonical treatment is a priori required to take into account exact strangeness conservation [18]. This approach leads to a dependence on system size as can be seen in p-Pb collisions studying multi-strange hadrons [10]. For the chosen ratios, however, the canonical corrections are identical for numerator and denominator (same strangeness quantum number). Therefore, the grand canonical values are used in Fig. 8 for two models [7,18], which are marked at the asymptotic limit, corresponding to the mean charged-particle multiplicity in Pb–Pb [43].

The constant behaviour of the yield ratios of excited to ground-state hyperons with same strangeness content indicates that neither regeneration nor re-scattering dominates with increasing collision system size, even for $\Sigma^{*\pm}$, which has a shorter lifetime than Ξ^{*0} by a factor of 4. It is especially interesting to consider the constant behaviour of $\Sigma^{*\pm}/\Lambda$ ratio in contrast to the apparent decrease observed for $\rm K^{*0}/K^-$ ratio in the same $\langle {\rm d}N_{\rm ch}/{\rm d}\eta_{\rm lab} \rangle$ range [14], in spite of the sim-

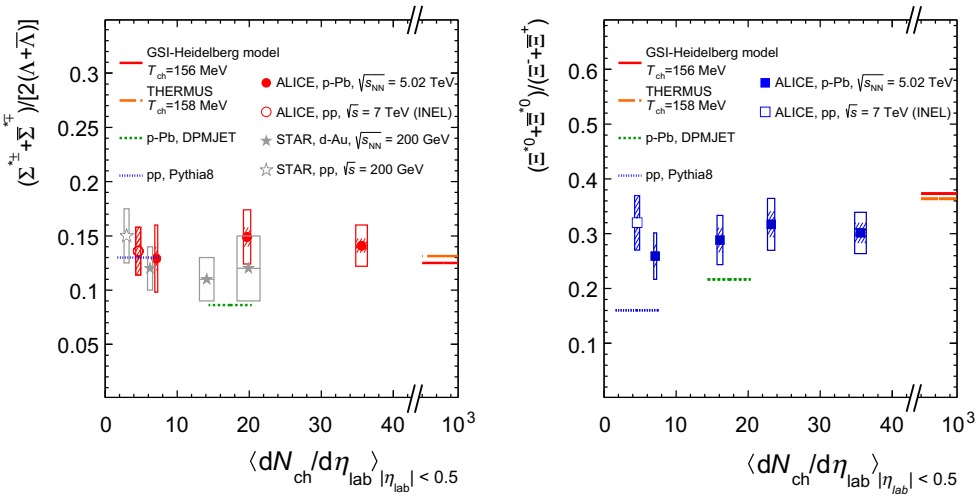

Fig. 8 (*Left*) ratio of $\Sigma^{*\pm}$ to Λ and (*Right*) ratio of Ξ^{*0} to Ξ^{-} measured in pp [17,32,37,39], d–Au [32,37] and p–Pb [10,24] collisions, as a function of $\langle dN_{ch}/d\eta_{lab}\rangle$ measured at midrapidity. Statistical uncertainties (*bars*) are shown as well as total systematic uncertainties (*hollow boxes*) and systematic uncertainties uncorrelated across multiplicity (*shaded boxes*). A few model predictions are also shown as *lines* at their appropriate abscissa

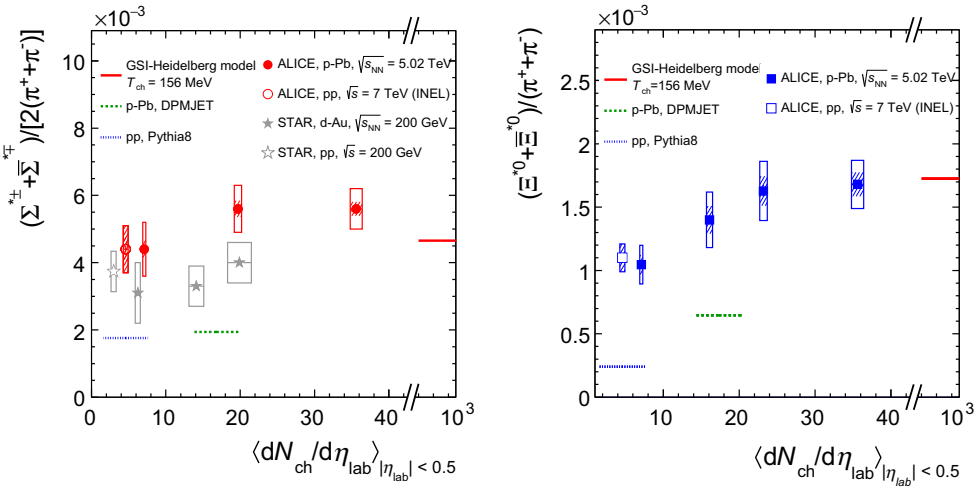

Fig. 9 (*Left*) ratio of $\Sigma^{*\pm}$ to $\pi^{\pm}$ and (*Right*) ratio of Ξ^{*0} to $\pi^{\pm}$, measured in pp [17,32,41,42], d–Au [32,37] and p–Pb [24] collisions, as a function of the average charged particle density ($\langle dN_{ch}/d\eta_{lab}\rangle$) measured at midrapidity. Statistical uncertainties (*bars*) are shown as well as total systematic uncertainties (*hollow boxes*) and systematic uncertainties uncorrelated across multiplicity (*shaded boxes*). A few model predictions are also shown as *lines* at their appropriate abscissa

ilarly short lifetimes of $\Sigma^{*\pm}$ and K^{*0}. In Pb–Pb collisions, both behaviours are predicted by the EPOS3 model [44,45], which employs the UrQMD model [46] for the description of the hadronic phase. In addition, the $\Sigma^{*\pm}/\Lambda$ ratios at LHC energies turn out to be comparable with the results obtained at lower energies by the STAR collaboration [32,37].

The integrated yield ratios of excited hyperons to pions are shown in Fig. 9 to study the evolution of relative strangeness production yields with increasing collision system size. Considering the relatively small systematic uncertainties uncorrelated across multiplicity (shaded boxes), one observes increasing patterns by 40–60% relative to results in pp collisions at the same $\sqrt{s_{NN}}$, depending on the strangeness contents. These results are consistent with previous observations of ground-state hyperons to pion ratios measured at ALICE [10]. The constant behavior of the $\Sigma^{*\pm}/\Lambda$ and Ξ^{*0}/Ξ^{-} ratios indicates that the strangeness enhancement observed in p-Pb collisions depends predominantly on the strangeness content, rather than on the hyperon mass. Results from low-energy collisions [32,37,42] show a similar pattern in spite of the narrower range accessible for mean charged-particle multiplicity. In both cases, QCD-inspired predictions like PYTHIA for pp [20] and DPMJET for p–Pb [19] clearly underestimate the observed yield ratios, while the statistical

one seems to be comparable with results from high multiplicity events.

5 Conclusions

Transverse momentum spectra of $\Sigma^{*\pm}$ and Ξ^{*0} produced in p–Pb collisions at $\sqrt{s_{\rm NN}} = 5.02$ TeV have been measured, and the yields and mean $p_{\rm T}$ values have been extracted with the help of Lévy–Tsallis fits. The mean $p_{\rm T}$ of these hyperon resonances exhibit a similarly increasing pattern as other hyperons (Λ, Ξ^-, Ω^-), depending on mean multiplicity and following the approximate mass ordering observed for other particles despite of relatively large uncertainties. The integrated yield ratios of excited to ground-state hyperons, with the same strangeness content, show a flat behaviour over the whole mean multiplicity range. The $\Sigma^{*\pm}/\Lambda$ ratio does not show a variation with collision energy, nor with increasing system size. The Ξ^{*0}/Ξ^- ratios are higher than predicted by event generators. Both ratios agree with thermal model values. The yield ratios relative to pions show a gradual increase with $\langle {\rm d}N_{\rm ch}/{\rm d}\eta_{\rm lab}\rangle$. This rise is consistent with the results of ground-state hyperons produced in the same collision system, i.e. they show a gradual evolution with the system size depending only on the strangeness content.

The current measurement represents a relevant baseline for further investigation in Pb–Pb collisions. It will be especially valuable to compare the $\Sigma^{*\pm}/\Lambda$ ratio with $\rm K^{*0}/K^-$, since $\Sigma^{*\pm}$ and $\rm K^{*0}$ have similar lifetimes. A complete set of such measurements for many resonances (ρ, $\rm K^{*0}$, ϕ, $\Sigma^{*\pm}$, Λ^*, Ξ^{*0}) with different lifetimes will allow the properties of the hadronic phase to be studied in more detail.

Acknowledgements The ALICE Collaboration would like to thank all its engineers and technicians for their invaluable contributions to the construction of the experiment and the CERN accelerator teams for the outstanding performance of the LHC complex. The ALICE Collaboration gratefully acknowledges the resources and support provided by all Grid centres and the Worldwide LHC Computing Grid (WLCG) collaboration. The ALICE Collaboration acknowledges the following funding agencies for their support in building and running the ALICE detector: A. I. Alikhanyan National Science Laboratory (Yerevan Physics Institute) Foundation (ANSL), State Committee of Science and World Federation of Scientists (WFS), Armenia; Austrian Academy of Sciences and Nationalstiftung für Forschung, Technologie und Entwicklung, Austria; Ministry of Communications and High Technologies, National Nuclear Research Center, Azerbaijan; Conselho Nacional de Desenvolvimento Científico e Tecnológico (CNPq), Universidade Federal do Rio Grande do Sul (UFRGS), Financiadora de Estudos e Projetos (Finep) and Fundação de Amparo à Pesquisa do Estado de São Paulo (FAPESP), Brazil; Ministry of Science & Technology of China (MSTC), National Natural Science Foundation of China (NSFC) and Ministry of Education of China (MOEC) , China; Ministry of Science, Education and Sport and Croatian Science Foundation, Croatia; Ministry of Education, Youth and Sports of the Czech Republic, Czech Republic; The Danish Council for Independent Research | Natural Sciences, the Carlsberg Foundation and Danish National Research Foundation (DNRF), Denmark; Helsinki Institute of Physics (HIP), Finland; Commissariat à l'Energie Atomique (CEA) and Institut National de Physique Nucléaire et de Physique des Particules (IN2P3) and Centre National de la Recherche Scientifique (CNRS), France; Bundesministerium für Bildung, Wissenschaft, Forschung und Technologie (BMBF) and GSI Helmholtzzentrum für Schwerionenforschung GmbH, Germany; Ministry of Education, Research and Religious Affairs, Greece; National Research, Development and Innovation Office, Hungary; Department of Atomic Energy Government of India (DAE) and Council of Scientific and Industrial Research (CSIR), New Delhi, India; Indonesian Institute of Science, Indonesia; Centro Fermi - Museo Storico della Fisica e Centro Studi e Ricerche Enrico Fermi and Istituto Nazionale di Fisica Nucleare (INFN), Italy; Institute for Innovative Science and Technology , Nagasaki Institute of Applied Science (IIST), Japan Society for the Promotion of Science (JSPS) KAKENHI and Japanese Ministry of Education, Culture, Sports, Science and Technology (MEXT), Japan; Consejo Nacional de Ciencia (CONACYT) y Tecnología, through Fondo de Cooperación Internacional en Ciencia y Tecnología (FONCICYT) and Dirección General de Asuntos del Personal Academico (DGAPA), Mexico; Nationaal instituut voor subatomaire fysica (Nikhef), Netherlands; The Research Council of Norway, Norway; Commission on Science and Technology for Sustainable Development in the South (COMSATS), Pakistan; Pontificia Universidad Católica del Perú, Peru; Ministry of Science and Higher Education and National Science Centre, Poland; Korea Institute of Science and Technology Information and National Research Foundation of Korea (NRF), Republic of Korea; Ministry of Education and Scientific Research, Institute of Atomic Physics and Romanian National Agency for Science, Technology and Innovation, Romania; Joint Institute for Nuclear Research (JINR), Ministry of Education and Science of the Russian Federation and National Research Centre Kurchatov Institute, Russia; Ministry of Education, Science, Research and Sport of the Slovak Republic, Slovakia; National Research Foundation of South Africa, South Africa; Centro de Aplicaciones Tecnológicas y Desarrollo Nuclear (CEADEN), Cubaenergía, Cuba, Ministerio de Ciencia e Innovacion and Centro de Investigaciones Energéticas, Medioambientales y Tecnológicas (CIEMAT), Spain; Swedish Research Council (VR) and Knut & Alice Wallenberg Foundation (KAW), Sweden; European Organization for Nuclear Research, Switzerland; National Science and Technology Development Agency (NSDTA), Suranaree University of Technology (SUT) and Office of the Higher Education Commission under NRU project of Thailand, Thailand; Turkish Atomic Energy Agency (TAEK), Turkey; National Academy of Sciences of Ukraine, Ukraine; Science and Technology Facilities Council (STFC), United Kingdom; National Science Foundation of the United States of America (NSF) and United States Department of Energy, Office of Nuclear Physics (DOE NP), United States of America.

Funded by SCOAP[3].

References

1. J. Rafelski, B. Muller, Strangeness production in the quark-gluon plasma. Phys. Rev. Lett. **48**, 1066–1069 (1982). doi:10.1103/PhysRevLett.48.1066
2. C. Blume, C. Markert, Strange hadron production in heavy ion collisions from SPS to RHIC. Prog. Part. Nucl. Phys. **66**, 834–879 (2011). doi:10.1016/j.ppnp.2011.05.001. arXiv:1105.2798 [nucl-ex]

3. WA97 Collaboration, E. Andersen et al., Strangeness enhancement at mid-rapidity in Pb-Pb collisions at 158 A GeV/ c. Phys. Lett. B **449**, 401–406 (1999). doi:10.1016/S0370-2693(99)00140-9
4. NA49 Collaboration, S. Afanasiev et al., Ξ^- and $\overline{\Xi}^+$ production in central Pb-Pb collisions at 158 GeV/ c per nucleon. Phys. Lett. B **538**, 275–281 (2002). doi:10.1016/S0370-2693(02)01970-6
5. S.T.A.R. Collaboration, J. Adams et al., Multistrange baryon production in Au-Au collisions at $\sqrt{s_{\rm NN}}$ = 130 GeV. Phys. Rev. Lett. **92**, 182301 (2004). doi:10.1103/PhysRevLett.92.182301
6. ALICE Collaboration, B. Abelev et al., Multi-strange baryon production at mid-rapidity in Pb–Pb collisions at $\sqrt{s_{\rm NN}}$ = 2.76 TeV. Phys. Lett. B **728**, 216–227 (2014). doi10.1016/j.physletb.2013.11.048. arXiv:1307.5543 [nucl-ex]
7. A. Andronic, P. Braun-Munzinger, J. Stachel, Thermal hadron production in relativistic nuclear collisions: The hadron mass spectrum, the horn, and the QCD phase transition. Phys. Lett. B **673**, 142–145 (2009). doi10.1016/j.physletb.2009.02.014. arXiv:0812.1186 [nucl-th]
8. K. Redlich, A. Tounsi, Strangeness enhancement and energy dependence in heavy ion collisions. Eur. Phys. J. C **24**, 589–594 (2002). doi:10.1007/s10052-002-0983-1
9. I. Kraus, J. Cleymans, H. Oeschler, K. Redlich, Particle production in pp collisions and predictions for $\sqrt{s}$ = 14 TeV at the CERN Large Hadron Collider (LHC). Phys. Rev. C **79**, 014901 (2009). doi:10.1103/PhysRevC.79.014901
10. ALICE Collaboration, J. Adam et al., Multi-strange baryon production in p–Pb collisions at $\sqrt{s_{\rm NN}}$=5.02 TeV. Phys. Lett. B **758**, 389–401 (2016). doi:10.1016/j.physletb.2016.05.027. arXiv:1512.07227 [nucl-ex]
11. G. Torrieri, J. Rafelski, Strange hadron resonances as a signature of freeze-out dynamics. Phys. Lett. B **509**, 239–245 (2001). doi:10.1016/S0370-2693(01)00492-0. arXiv:hep-ph/0103149
12. M. Bleicher, J. Aichelin, Strange resonance production: probing chemical and thermal freezeout in relativistic heavy ion collisions. Phys. Lett. B. **530**, 81–87 (2002). doi:10.1016/S0370-2693(02)01334-5. arXiv:hep-ph/0201123
13. ALICE Collaboration, B. Abelev et al., Production of $K^*(892)^0$ and $\phi(1020)$ in pp collisions at $\sqrt{s_{\rm NN}}$ = 7 TeV. Eur. Phys. J. C **72**, 2183 (2012). doi:10.1140/epjc/s10052-012-2183-y. arXiv:1208.5717 [nucl-ex]
14. ALICE Collaboration, J. Adam et al., Production of $K^*(892)^0$ and $\phi(1020)$ in p–Pb collisions at $\sqrt{s_{\rm NN}}$ = 5.02 TeV. Eur. Phys. J. C **76**, 245 (2016). doi:10.1140/epjc/s10052-016-4088-7. arXiv:1601.7868 [nucl-ex]
15. ALICE Collaboration, B. Abelev et al., $K^*(892)^0$ and $\phi(1020)$ production in Pb–Pb collisions at $\sqrt{s_{\rm NN}}$ = 2.76 TeV. Phys. Rev. C **91**, 024609 (2015). doi:10.1103/PhysRevC.91.024609. arXiv:1404.0495 [nucl-ex]
16. Particle Data Group Collaboration, K. Olive et al., Review of Particle Physics. Chin. Phys. C **38**, 090001 (2014). doi:10.1088/1674-1137/38/9/090001
17. ALICE Collaboration, B. Abelev et al., Production of $\Sigma(1385)^{\pm}$ and $\Xi(1530)^0$ in proton-proton collisions at $\sqrt{s}$ = 7 TeV. Eur. Phys. J. C **75**, 1 (2015). doi10.1140/epjc/s10052-014-3191-x. arXiv:1406.3206 [nucl-ex]
18. S. Wheaton, J. Cleymans, M. Hauer, THERMUS—a thermal model package for ROOT. Comput. Phys. Commun. **180**, 84–106 (2009). doi:10.1016/j.cpc.2008.08.001
19. S. Roesler, R. Engel, J. Ranft, The Monte Carlo event generator DPMJET-III, advanced Monte Carlo for radiation physics, particle transport simulation and applications. in *Conference Proceedings, MC2000, Lisbon, Portugal, October 23–26*, pp. 1033–1038 (2000). doi:10.1007/978-3-642-18211-2_166. arXiv:hep-ph/0012252
20. T. Sjöstrand, S. Mrenna, P. Skands, A brief introduction to PYTHIA 8.1. Comput. Phys. Commun. **178**, 852–867 (2008). doi:10.1016/j.cpc.2008.01.036. arXiv:0710.3820 [hep-ph]
21. ALICE Collaboration, K. Aamodt et al., The ALICE experiment at the CERN LHC. JINST **3**, S08002 (2008). doi:10.1088/1748-0221/3/08/S08002
22. ALICE Collaboration, B. Abelev et al., Performance of the ALICE Experiment at the CERN LHC. Int. J. Mod. Phys. A **29**, 1430044 (2014). doi:10.1142/S0217751X14300440. arXiv:1402.4476 [nucl-ex]
23. ALICE Collaboration, B. Abelev et al., Pseudorapidity density of charged particles in p–Pb collisions at $\sqrt{s_{\rm NN}}$ = 5.02 TeV. Phys. Rev. Lett. **110**, 032301 (2013). doi:10.1103/PhysRevLett.110.032301. arXiv:1210.3615 [nucl-ex]
24. ALICE Collaboration, J. Adam et al., Multiplicity dependence of pion, kaon, proton and lambda production in p–Pb collisions at $\sqrt{s_{\rm NN}}$ = 5.02 TeV. Phys. Lett. B **728**, 25–38 (2014). doi:10.1016/j.physletb.2013.11.020. arXiv:1307.6796 [nucl-ex]
25. ALICE Collaboration, J. Adam et al., Centrality dependence of particle production in p–Pb collisions at $\sqrt{s_{\rm NN}}$= 5.02 TeV. Phys. Rev. C **91**, 064905 (2015). doi:10.1103/PhysRevC.91.064905. arXiv:1412.6828 [nucl-ex]
26. ALICE Collaboration, K. Aamodt et al., Strange particle production in proton-proton collisions at $\sqrt{s}$ = 0.9 TeV with ALICE at the LHC. *Eur. Phys. J. C***71**, 1594 (2011). doi:10.1140/epjc/s10052-011-1594-5. arXiv:1012.3257 [nucl-ex]
27. R. Brun, F. Carminati, S. Giani, GEANT detector description and simulation tool. CERN-W5013 (1994)
28. ALICE Collaboration, K. Aamodt et al., Midrapidity antiproton-to-proton ratio in pp collisions at $\sqrt{s}$ = 0.9 and 7 TeV measured by the ALICE experiment. Phys. Rev. Lett. **105**, 072002 (2010). doi:10.1103/PhysRevLett.105.072002. arXiv:1006.5432 [hep-ex]
29. R. Barlow, Systematic errors: facts and fictions. Presented at Advanced Statistical Techniques in HEP, Durham, March 2002, p. 333 (2002). arXiv:hep-ex/0207026v1
30. C. Tsallis, Possible generalization of Boltzmann-Gibbs statistics. J. Stat. Phys. **52**, 479–487 (1988). doi:10.1007/BF01016429
31. E. Schnedermann, J. Sollfrank, U. Heinz, Thermal phenomenology of hadrons from 200*A* GeV S+S collisions. Phys. Rev. C **48**, 2462–2475 (1993). doi:10.1103/PhysRevC.48.2462. arXiv:nucl-th/9307020
32. STAR Collaboration, B.I. Abelev et al., Systematic measurements of identified particle spectra in pp, d-Au, and Au-Au collisions at the STAR detector. Phys. Rev. C **79**, 034909 (2009). doi:10.1103/PhysRevC.79.034909
33. STAR Collaboration, J. Adams et al., K(892)* resonance production in Au-Au and pp collisions at $\sqrt{s_{\rm NN}}$ = 200 GeV. Phys. Rev. C **71**, 064902 (2005). doi:10.1103/PhysRevC.71.064902. arXiv:nucl-ex/0412019v2
34. ALICE Collaboration, J. Adam et al., *D*-meson production in p–Pb collisions at $\sqrt{s_{\rm NN}}$ = 5.02 TeV and in pp collisions at $\sqrt{s}$ = 7 TeV. *Phys. Rev. C***94**, 054908 (2016). doi:10.1103/PhysRevC.94.054908. arXiv:1605.07569 [nucl-ex]
35. ALICE Collaboration, B. Abelev et al., Inclusive J/ψ production in pp collisions at $\sqrt{s}$ = 2.76 TeV. Phys. Lett. B **718**, 295–306 (2012). doi:10.1016/j.physletb.2012.10.078. arXiv:1203.3641 [hep-ex]
36. ALICE Collaboration, J. Adam et al., Rapidity and transverse-momentum dependence of the inclusive J/ψ nuclear modification factor in p–Pb collisions at $\sqrt{s_{\rm NN}}$ = 5.02 TeV. JHEP**06**, 55 (2015). doi:10.1007/JHEP06(2015)055. arXiv:1503.07179 [nucl-ex]
37. STAR Collaboration, B.I. Abelev et al., Hadronic resonance production in d-Au collisions at $\sqrt{s_{\rm NN}}$ = 200 GeV measured at the BNL Relativistic Heavy-Ion Collider. Phys. Rev. C **78**, 044906 (2008). doi:10.1103/PhysRevC.78.044906. arXiv:0801.0450 [nucl-ex]

38. A. Velásquez, Mean p_T scaling with m/n_q at the LHC: Absence of (hydro) flow in small systems? Nucl. Phys. A **943**, 9–17 (2015). doi:10.1016/j.nuclphysa.2015.08.003. arXiv:1506.00584 [hep-ph]
39. ALICE Collaboration, B. Abelev et al., Multi-strange baryon production in pp collisions at $\sqrt{s}$ = 7 TeV with ALICE. Phys. Lett. B **712**, 309 (2012). doi:10.1016/j.physletb.2012.05.011. arXiv:1204.0282 [nucl-ex]
40. ALICE Collaboration, J. Adam et al., Charged-particle multiplicities in proton-proton collisions at $\sqrt{s}$ = 0.9 to 8 TeV. arXiv:1509.07541 [nucl-ex]
41. ALICE Collaboration, J. Adam et al., Measurement of pion, kaon and proton production in proton-proton collisions at $\sqrt{s}$ = 7 TeV. Eur. Phys. J. C **75**, 226 (2015). doi:10.1140/epjc/s10052-015-3422-9. arXiv:1504.00024 [nucl-ex]
42. STAR Collaboration, B.I. Abelev et al., Strange baryon resonance production in $\sqrt{s_{NN}}$ = 200GeV p+p and Au+Au collisions. Phys. Rev. Lett. **97**, 132301 (2006). doi:10.1103/PhysRevLett.97.132301. arXiv:nucl-ex/0604019v2
43. ALICE Collaboration, J. Adam et al., Centrality Dependence of the Charged-Particle Multiplicity Density at Midrapidity in Pb–Pb Collisions at 5.02 TeV $\sqrt{s_{NN}}$ = 5.02 TeV. Phys. Rev. Lett. **116**, 222302 (2010). doi:10.1103/PhysRevLett.116.222302. arXiv:1512.06104 [hep-ex]
44. K. Werner, B. Guiot, I. Karpenko, T. Pierog, Analyzing radial flow features in p-Pb and p-p collisions at several TeV by studying identified-particle production with the event generator EPOS3. Phys. Rev. C **89**, 064903 (2014). doi:10.1103/PhysRevC.89.064903
45. A. Knospe, C. Markert, K. Werner, J. Steinheimer, M. Bleicher, Hadronic resonance production and interaction in partonic and hadronic matter in the EPOS3 model with and without the hadronic afterburner UrQMD. Phys. Rev. C **93**, 014911 (2016). doi:10.1103/PhysRevC.93.014911
46. M. Bleicher et al., Relativistic hadron-hadron collisions in the ultra-relativistic quantum molecular dynamics model. J. Phys. G. **25**, 1859 (1999). doi:10.1016/S0370-2693(02)01334-5

ALICE Collaboration

D. Adamová[87], M. M. Aggarwal[91], G. Aglieri Rinella[34], M. Agnello[30,113], N. Agrawal[47], Z. Ahammed[139], S. Ahmad[17], S. U. Ahn[69], S. Aiola[143], A. Akindinov[54], S. N. Alam[139], D. S. D. Albuquerque[124], D. Aleksandrov[83], B. Alessandro[113], D. Alexandre[104], R. Alfaro Molina[64], A. Alici[12,107], A. Alkin[3], J. Alme[21,36], T. Alt[41], S. Altinpinar[21], I. Altsybeev[138], C. Alves Garcia Prado[123], M. An[7], C. Andrei[80], H. A. Andrews[104], A. Andronic[100], V. Anguelov[96], C. Anson[90], T. Antičić[101], F. Antinori[110], P. Antonioli[107], R. Anwar[126], L. Aphecetche[116], H. Appelshäuser[60], S. Arcelli[26], R. Arnaldi[113], O. W. Arnold[35,97], I. C. Arsene[20], M. Arslandok[60], B. Audurier[116], A. Augustinus[34], R. Averbeck[100], M. D. Azmi[17], A. Badalà[109], Y. W. Baek[68], S. Bagnasco[113], R. Bailhache[60], R. Bala[93], A. Baldisseri[65], M. Ball[44], R. C. Baral[57], A. M. Barbano[25], R. Barbera[27], F. Barile[32], L. Barioglio[25], G. G. Barnaföldi[142], L. S. Barnby[34,104], V. Barret[71], P. Bartalini[7], K. Barth[34], J. Bartke[120,a], E. Bartsch[60], M. Basile[26], N. Bastid[71], S. Basu[139], B. Bathen[61], G. Batigne[116], A. Batista Camejo[71], B. Batyunya[67], P. C. Batzing[20], I. G. Bearden[84], H. Beck[96], C. Bedda[30], N. K. Behera[50], I. Belikov[135], F. Bellini[26], H. Bello Martinez[2], R. Bellwied[126], L. G. E. Beltran[122], V. Belyaev[76], G. Bencedi[142], S. Beole[25], A. Bercuci[80], Y. Berdnikov[89], D. Berenyi[142], R. A. Bertens[53,129], D. Berzano[34], L. Betev[34], A. Bhasin[93], I. R. Bhat[93], A. K. Bhati[91], B. Bhattacharjee[43], J. Bhom[120], L. Bianchi[126], N. Bianchi[73], C. Bianchin[141], J. Bielčík[38], J. Bielčíková[87], A. Bilandzic[35,97], G. Biro[142], R. Biswas[4], S. Biswas[4], J. T. Blair[121], D. Blau[83], C. Blume[60], G. Boca[136], F. Bock[75,96], A. Bogdanov[76], L. Boldizsár[142], M. Bombara[39], G. Bonomi[137], M. Bonora[34], J. Book[60], H. Borel[65], A. Borissov[99], M. Borri[128], E. Botta[25], C. Bourjau[84], P. Braun-Munzinger[100], M. Bregant[123], T. A. Broker[60], T. A. Browning[98], M. Broz[38], E. J. Brucken[45], E. Bruna[113], G. E. Bruno[32], D. Budnikov[102], H. Buesching[60], S. Bufalino[30,25], P. Buhler[115], S. A. I. Buitron[62], P. Buncic[34], O. Busch[132], Z. Buthelezi[66], J. B. Butt[15], J. T. Buxton[18], J. Cabala[118], D. Caffarri[34], H. Caines[143], A. Caliva[53], E. Calvo Villar[105], P. Camerini[24], A. A. Capon[115], F. Carena[34], W. Carena[34], F. Carnesecchi[26,12], J. Castillo Castellanos[65], A. J. Castro[129], E. A. R. Casula[23,108], C. Ceballos Sanchez[9], P. Cerello[113], B. Chang[127], S. Chapeland[34], M. Chartier[128], J. L. Charvet[65], S. Chattopadhyay[139], S. Chattopadhyay[103], A. Chauvin[35,97], M. Cherney[90], C. Cheshkov[134], B. Cheynis[134], V. Chibante Barroso[34], D. D. Chinellato[124], S. Cho[50], P. Chochula[34], K. Choi[99], M. Chojnacki[84], S. Choudhury[139], P. Christakoglou[85], C. H. Christensen[84], P. Christiansen[33], T. Chujo[132], S. U. Chung[99], C. Cicalo[108], L. Cifarelli[12,26], F. Cindolo[107], J. Cleymans[92], F. Colamaria[32], D. Colella[34,55], A. Collu[75], M. Colocci[26], G. Conesa Balbastre[72], Z. Conesa del Valle[51], M. E. Connors[143,b], J. G. Contreras[38], T. M. Cormier[88], Y. Corrales Morales[113], I. Cortés Maldonado[2], P. Cortese[31], M. R. Cosentino[125], F. Costa[34], S. Costanza[136], J. Crkovská[51], P. Crochet[71], E. Cuautle[62], L. Cunqueiro[61], T. Dahms[35,97], A. Dainese[110], M. C. Danisch[96], A. Danu[58], D. Das[103], I. Das[103], S. Das[4], A. Dash[81], S. Dash[47], S. De[48,123], A. De Caro[29], G. de Cataldo[106], C. de Conti[123], J. de Cuveland[41], A. De Falco[23], D. De Gruttola[12,29], N. De Marco[113], S. De Pasquale[29], R. D. De Souza[124], H. F. Degenhardt[123], A. Deisting[96,100], A. Deloff[79], C. Deplano[85], P. Dhankher[47], D. Di Bari[32], A. Di Mauro[34], P. Di Nezza[73], B. Di Ruzza[110], M. A. Diaz Corchero[10], T. Dietel[92], P. Dillenseger[60], R. Divià[34], Ø. Djuvsland[21], A. Dobrin[34,58], D. Domenicis Gimenez[123], B. Dönigus[60], O. Dordic[20], T. Drozhzhova[60], A. K. Dubey[139], A. Dubla[100], L. Ducroux[134], A. K. Duggal[91], P. Dupieux[71], R. J. Ehlers[143], D. Elia[106], E. Endress[105], H. Engel[59], E. Epple[143], B. Erazmus[116], F. Erhardt[133], B. Espagnon[51], S. Esumi[132], G. Eulisse[34], J. Eum[99], D. Evans[104], S. Evdokimov[114], L. Fabbietti[35,97], D. Fabris[110], J. Faivre[72],

A. Fantoni[73], M. Fasel[75,88], L. Feldkamp[61], A. Feliciello[113], G. Feofilov[138], J. Ferencei[87], A. Fernández Téllez[2], E. G. Ferreiro[16], A. Ferretti[25], A. Festanti[28], V. J. G. Feuillard[65,71], J. Figiel[120], M. A. S. Figueredo[123], S. Filchagin[102], D. Finogeev[52], F. M. Fionda[23], E. M. Fiore[32], M. Floris[34], S. Foertsch[66], P. Foka[100], S. Fokin[83], E. Fragiacomo[112], A. Francescon[34], A. Francisco[116], U. Frankenfeld[100], G. G. Fronze[25], U. Fuchs[34], C. Furget[72], A. Furs[52], M. Fusco Girard[29], J. J. Gaardhøje[84], M. Gagliardi[25], A. M. Gago[105], K. Gajdosova[84], M. Gallio[25], C. D. Galvan[122], D. R. Gangadharan[75], P. Ganoti[78], C. Gao[7], C. Garabatos[100], E. Garcia-Solis[13], K. Garg[27], P. Garg[48], C. Gargiulo[34], P. Gasik[35,97], E. F. Gauger[121], M. B. Gay Ducati[63], M. Germain[116], P. Ghosh[139], S. K. Ghosh[4], P. Gianotti[73], P. Giubellino[34,113], P. Giubilato[28], E. Gladysz-Dziadus[120], P. Glässel[96], D. M. Goméz Coral[64], A. Gomez Ramirez[59], A. S. Gonzalez[34], V. Gonzalez[10], P. González-Zamora[10], S. Gorbunov[41], L. Görlich[120], S. Gotovac[119], V. Grabski[64], L. K. Graczykowski[140], K. L. Graham[104], L. Greiner[75], A. Grelli[53], C. Grigoras[34], V. Grigoriev[76], A. Grigoryan[1], S. Grigoryan[67], N. Grion[112], J. M. Gronefeld[100], F. Grosa[30], J. F. Grosse-Oetringhaus[34], R. Grosso[100], L. Gruber[115], F. R. Grull[59], F. Guber[52], R. Guernane[34,72], B. Guerzoni[26], K. Gulbrandsen[84], T. Gunji[131], A. Gupta[93], R. Gupta[93], I. B. Guzman[2], R. Haake[34,61], C. Hadjidakis[51], H. Hamagaki[77,131], G. Hamar[142], J. C. Hamon[135], J. W. Harris[143], A. Harton[13], D. Hatzifotiadou[107], S. Hayashi[131], S. T. Heckel[60], E. Hellbär[60], H. Helstrup[36], A. Herghelegiu[80], G. Herrera Corral[11], F. Herrmann[61], B. A. Hess[95], K. F. Hetland[36], H. Hillemanns[34], B. Hippolyte[135], J. Hladky[56], D. Horak[38], R. Hosokawa[132], P. Hristov[34], C. Hughes[129], T. J. Humanic[18], N. Hussain[43], T. Hussain[17], D. Hutter[41], D. S. Hwang[19], R. Ilkaev[102], M. Inaba[132], M. Ippolitov[76,83], M. Irfan[17], V. Isakov[52], M. S. Islam[48], M. Ivanov[34,100], V. Ivanov[89], V. Izucheev[114], B. Jacak[75], N. Jacazio[26], P. M. Jacobs[75], M. B. Jadhav[47], S. Jadlovska[118], J. Jadlovsky[118], C. Jahnke[35], M. J. Jakubowska[140], M. A. Janik[140], P. H. S. Y. Jayarathna[126], C. Jena[81], S. Jena[126], M. Jercic[133], R. T. Jimenez Bustamante[100], P. G. Jones[104], A. Jusko[104], P. Kalinak[55], A. Kalweit[34], J. H. Kang[144], V. Kaplin[76], S. Kar[139], A. Karasu Uysal[70], O. Karavichev[52], T. Karavicheva[52], L. Karayan[96,100], E. Karpechev[52], U. Kebschull[59], R. Keidel[145], D. L. D. Keijdener[53], M. Keil[34], B. Ketzer[44], M. Mohisin Khan[17,c], P. Khan[103], S. A. Khan[139], A. Khanzadeev[89], Y. Kharlov[114], A. Khatun[17], A. Khuntia[48], M. M. Kielbowicz[120], B. Kileng[36], D. W. Kim[42], D. J. Kim[127], D. Kim[144], H. Kim[144], J. S. Kim[42], J. Kim[96], M. Kim[50], M. Kim[144], S. Kim[19], T. Kim[144], S. Kirsch[41], I. Kisel[41], S. Kiselev[54], A. Kisiel[140], G. Kiss[142], J. L. Klay[6], C. Klein[60], J. Klein[34], C. Klein-Bösing[61], S. Klewin[96], A. Kluge[34], M. L. Knichel[96], A. G. Knospe[126], C. Kobdaj[117], M. Kofarago[34], T. Kollegger[100], A. Kolojvari[138], V. Kondratiev[138], N. Kondratyeva[76], E. Kondratyuk[114], A. Konevskikh[52], M. Kopcik[118], M. Kour[93], C. Kouzinopoulos[34], O. Kovalenko[79], V. Kovalenko[138], M. Kowalski[120], G. Koyithatta Meethaleveedu[47], I. Králik[55], A. Kravčáková[39], M. Krivda[55,104], F. Krizek[87], E. Kryshen[89], M. Krzewicki[41], A. M. Kubera[18], V. Kučera[87], C. Kuhn[135], P. G. Kuijer[85], A. Kumar[93], J. Kumar[47], L. Kumar[91], S. Kumar[47], S. Kundu[81], P. Kurashvili[79], A. Kurepin[52], A. B. Kurepin[52], A. Kuryakin[102], S. Kushpil[87], M. J. Kweon[50], Y. Kwon[144], S. L. La Pointe[41], P. La Rocca[27], C. Lagana Fernandes[123], I. Lakomov[34], R. Langoy[40], K. Lapidus[143], C. Lara[59], A. Lardeux[20,65], A. Lattuca[25], E. Laudi[34], R. Lavicka[38], L. Lazaridis[34], R. Lea[24], L. Leardini[96], S. Lee[144], F. Lehas[85], S. Lehner[115], J. Lehrbach[41], R. C. Lemmon[86], V. Lenti[106], E. Leogrande[53], I. León Monzón[122], P. Lévai[142], S. Li[7], X. Li[14], J. Lien[40], R. Lietava[104], S. Lindal[20], V. Lindenstruth[41], C. Lippmann[100], M. A. Lisa[18], V. Litichevskyi[45], H. M. Ljunggren[33], W. J. Llope[141], D. F. Lodato[53], P. I. Loenne[21], V. Loginov[76], C. Loizides[75], P. Loncar[119], X. Lopez[71], E. López Torres[9], A. Lowe[142], P. Luettig[60], M. Lunardon[28], G. Luparello[24], M. Lupi[34], T. H. Lutz[143], A. Maevskaya[52], M. Mager[34], S. Mahajan[93], S. M. Mahmood[20], A. Maire[135], R. D. Majka[143], M. Malaev[89], I. Maldonado Cervantes[62], L. Malinina[67,d], D. Mal'Kevich[54], P. Malzacher[100], A. Mamonov[102], V. Manko[83], F. Manso[71], V. Manzari[106], Y. Mao[7], M. Marchisone[66,130], J. Mareš[56], G. V. Margagliotti[24], A. Margotti[107], J. Margutti[53], A. Marín[100], C. Markert[121], M. Marquard[60], N. A. Martin[100], P. Martinengo[34], J. A. L. Martinez[59], M. I. Martínez[2], G. Martínez García[116], M. Martinez Pedreira[34], A. Mas[123], S. Masciocchi[100], M. Masera[25], A. Masoni[108], A. Mastroserio[32], A. M. Mathis[35,97], A. Matyja[120,129], C. Mayer[120], J. Mazer[129], M. Mazzilli[32], M. A. Mazzoni[111], F. Meddi[22], Y. Melikyan[76], A. Menchaca-Rocha[64], E. Meninno[29], J. Mercado Pérez[96], M. Meres[37], S. Mhlanga[92], Y. Miake[132], M. M. Mieskolainen[45], D. Mihaylov[97], K. Mikhaylov[54,67], L. Milano[75], J. Milosevic[20], A. Mischke[53], A. N. Mishra[48], D. Miśkowiec[100], J. Mitra[139], C. M. Mitu[58], N. Mohammadi[53], B. Mohanty[81], E. Montes[10], D. A. Moreira De Godoy[61], L. A. P. Moreno[2], S. Moretto[28], A. Morreale[116], A. Morsch[34], V. Muccifora[73], E. Mudnic[119], D. Mühlheim[61], S. Muhuri[139], M. Mukherjee[139], J. D. Mulligan[143], M. G. Munhoz[123], K. Münning[44], R. H. Munzer[35,60,97], H. Murakami[131], S. Murray[66], L. Musa[34], J. Musinsky[55], C. J. Myers[126], B. Naik[47], R. Nair[79], B. K. Nandi[47], R. Nania[107], E. Nappi[106], M. U. Naru[15], H. Natal da Luz[123], C. Nattrass[129], S. R. Navarro[2], K. Nayak[81], R. Nayak[47], T. K. Nayak[139], S. Nazarenko[102], A. Nedosekin[54], R. A. Negrao De Oliveira[34], L. Nellen[62], S. V. Nesbo[36], F. Ng[126], M. Nicassio[100], M. Niculescu[58], J. Niedziela[34], B. S. Nielsen[84], S. Nikolaev[83], S. Nikulin[83], V. Nikulin[89], F. Noferini[12,107], P. Nomokonov[67], G. Nooren[53], J. C. C. Noris[2], J. Norman[128], A. Nyanin[83], J. Nystrand[21], H. Oeschler[96], S. Oh[143], A. Ohlson[34,96], T. Okubo[46], L. Olah[142], J. Oleniacz[140], A. C. Oliveira Da Silva[123], M. H. Oliver[143], J. Onderwaater[100], C. Oppedisano[113], R. Orava[45], M. Oravec[118], A. Ortiz Velasquez[62], A. Oskarsson[33],

J. Otwinowski[120], K. Oyama[77], M. Ozdemir[60], Y. Pachmayer[96], V. Pacik[84], D. Pagano[137], P. Pagano[29], G. Paić[62], S. K. Pal[139], P. Palni[7], J. Pan[141], A. K. Pandey[47], S. Panebianco[65], V. Papikyan[1], G. S. Pappalardo[109], P. Pareek[48], J. Park[50], W. J. Park[100], S. Parmar[91], A. Passfeld[61], S. P. Pathak[126], V. Paticchio[106], R. N. Patra[139], B. Paul[113], H. Pei[7], T. Peitzmann[53], X. Peng[7], L. G. Pereira[63], H. Pereira Da Costa[65], D. Peresunko[76,83], E. Perez Lezama[60], V. Peskov[60], Y. Pestov[5], V. Petráček[38], V. Petrov[114], M. Petrovici[80], C. Petta[27], R. P. Pezzi[63], S. Piano[112], M. Pikna[37], P. Pillot[116], L. O. D. L. Pimentel[84], O. Pinazza[34,107], L. Pinsky[126], D. B. Piyarathna[126], M. Płoskoń[75], M. Planinic[133], J. Pluta[140], S. Pochybova[142], P. L. M. Podesta-Lerma[122], M. G. Poghosyan[88], B. Polichtchouk[114], N. Poljak[133], W. Poonsawat[117], A. Pop[80], H. Poppenborg[61], S. Porteboeuf-Houssais[71], J. Porter[75], J. Pospisil[87], V. Pozdniakov[67], S. K. Prasad[4], R. Preghenella[34,107], F. Prino[113], C. A. Pruneau[141], I. Pshenichnov[52], M. Puccio[25], G. Puddu[23], P. Pujahari[141], V. Punin[102], J. Putschke[141], H. Qvigstad[20], A. Rachevski[112], S. Raha[4], S. Rajput[93], J. Rak[127], A. Rakotozafindrabe[65], L. Ramello[31], F. Rami[135], D. B. Rana[126], R. Raniwala[94], S. Raniwala[94], S. S. Räsänen[45], B. T. Rascanu[60], D. Rathee[91], V. Ratza[44], I. Ravasenga[30], K. F. Read[88,129], K. Redlich[79], A. Rehman[21], P. Reichelt[60], F. Reidt[34], X. Ren[7], R. Renfordt[60], A. R. Reolon[73], A. Reshetin[52], K. Reygers[96], V. Riabov[89], R. A. Ricci[74], T. Richert[53,33], M. Richter[20], P. Riedler[34], W. Riegler[34], F. Riggi[27], C. Ristea[58], M. Rodríguez Cahuantzi[2], K. Røed[20], E. Rogochaya[67], D. Rohr[41], D. Röhrich[21], P. S. Rokita[140], F. Ronchetti[34,73], L. Ronflette[116], P. Rosnet[71], A. Rossi[28], A. Rotondi[136], F. Roukoutakis[78], A. Roy[48], C. Roy[135], P. Roy[103], A. J. Rubio Montero[10], R. Rui[24], R. Russo[25], A. Rustamov[82], E. Ryabinkin[83], Y. Ryabov[89], A. Rybicki[120], S. Saarinen[45], S. Sadhu[139], S. Sadovsky[114], K. Šafařík[34], S. K. Saha[139], B. Sahlmuller[60], B. Sahoo[47], P. Sahoo[48], R. Sahoo[48], S. Sahoo[57], P. K. Sahu[57], J. Saini[139], S. Sakai[73,132], M. A. Saleh[141], J. Salzwedel[18], S. Sambyal[93], V. Samsonov[76,89], A. Sandoval[64], D. Sarkar[139], N. Sarkar[139], P. Sarma[43], M. H. P. Sas[53], E. Scapparone[107], F. Scarlassara[28], R. P. Scharenberg[98], H. S. Scheid[60], C. Schiaua[80], R. Schicker[96], C. Schmidt[100], H. R. Schmidt[95], M. O. Schmidt[96], M. Schmidt[95], J. Schukraft[34], Y. Schutz[34,116,135], K. Schwarz[100], K. Schweda[100], G. Scioli[26], E. Scomparin[113], R. Scott[129], M. Šefčík[39], J. E. Seger[90], Y. Sekiguchi[131], D. Sekihata[46], I. Selyuzhenkov[100], K. Senosi[66], S. Senyukov[3,34,135], E. Serradilla[64,10], P. Sett[47], A. Sevcenco[58], A. Shabanov[52], A. Shabetai[116], O. Shadura[3], R. Shahoyan[34], A. Shangaraev[114], A. Sharma[93], A. Sharma[91], M. Sharma[93], M. Sharma[93], N. Sharma[91,129], A. I. Sheikh[139], K. Shigaki[46], Q. Shou[7], K. Shtejer[9,25], Y. Sibiriak[83], S. Siddhanta[108], K. M. Sielewicz[34], T. Siemiarczuk[79], D. Silvermyr[33], C. Silvestre[72], G. Simatovic[133], G. Simonetti[34], R. Singaraju[139], R. Singh[81], V. Singhal[139], T. Sinha[103], B. Sitar[37], M. Sitta[31], T. B. Skaali[20], M. Slupecki[127], N. Smirnov[143], R. J. M. Snellings[53], T. W. Snellman[127], J. Song[99], M. Song[144], F. Soramel[28], S. Sorensen[129], F. Sozzi[100], E. Spiriti[73], I. Sputowska[120], B. K. Srivastava[98], J. Stachel[96], I. Stan[58], P. Stankus[88], E. Stenlund[33], J. H. Stiller[96], D. Stocco[116], P. Strmen[37], A. A. P. Suaide[123], T. Sugitate[46], C. Suire[51], M. Suleymanov[15], M. Suljic[24], R. Sultanov[54], M. Šumbera[87], S. Sumowidagdo[49], K. Suzuki[115], S. Swain[57], A. Szabo[37], I. Szarka[37], A. Szczepankiewicz[140], M. Szymanski[140], U. Tabassam[15], J. Takahashi[124], G. J. Tambave[21], N. Tanaka[132], M. Tarhini[51], M. Tariq[17], M. G. Tarzila[80], A. Tauro[34], G. Tejeda Muñoz[2], A. Telesca[34], K. Terasaki[131], C. Terrevoli[28], B. Teyssier[134], D. Thakur[48], S. Thakur[139], D. Thomas[121], R. Tieulent[134], A. Tikhonov[52], A. R. Timmins[126], A. Toia[60], S. Tripathy[48], S. Trogolo[25], G. Trombetta[32], V. Trubnikov[3], W. H. Trzaska[127], B. A. Trzeciak[53], T. Tsuji[131], A. Tumkin[102], R. Turrisi[110], T. S. Tveter[20], K. Ullaland[21], E. N. Umaka[126], A. Uras[134], G. L. Usai[23], A. Utrobicic[133], M. Vala[55,118], J. Van Der Maarel[53], J. W. Van Hoorne[34], M. van Leeuwen[53], T. Vanat[87], P. Vande Vyvre[34], D. Varga[142], A. Vargas[2], M. Vargyas[127], R. Varma[47], M. Vasileiou[78], A. Vasiliev[83], A. Vauthier[72], O. Vázquez Doce[35,97], V. Vechernin[138], A. M. Veen[53], A. Velure[21], E. Vercellin[25], S. Vergara Limón[2], R. Vernet[8], R. Vértesi[142], L. Vickovic[119], S. Vigolo[53], J. Viinikainen[127], Z. Vilakazi[130], O. Villalobos Baillie[104], A. Villatoro Tello[2], A. Vinogradov[83], L. Vinogradov[138], T. Virgili[29], V. Vislavicius[33], A. Vodopyanov[67], M. A. Völkl[96], K. Voloshin[54], S. A. Voloshin[141], G. Volpe[32], B. von Haller[34], I. Vorobyev[35,97], D. Voscek[118], D. Vranic[34,100], J. Vrláková[39], B. Wagner[21], J. Wagner[100], H. Wang[53], M. Wang[7], D. Watanabe[132], Y. Watanabe[131], M. Weber[115], S. G. Weber[100], D. F. Weiser[96], J. P. Wessels[61], U. Westerhoff[61], A. M. Whitehead[92], J. Wiechula[60], J. Wikne[20], G. Wilk[79], J. Wilkinson[96], G. A. Willems[61], M. C. S. Williams[107], B. Windelband[96], W. E. Witt[129], S. Yalcin[70], P. Yang[7], S. Yano[46], Z. Yin[7], H. Yokoyama[72,132], I.-K. Yoo[34,99], J. H. Yoon[50], V. Yurchenko[3], V. Zaccolo[84,113], A. Zaman[15], C. Zampolli[34], H. J. C. Zanoli[123], S. Zaporozhets[67], N. Zardoshti[104], A. Zarochentsev[138], P. Závada[56], N. Zaviyalov[102], H. Zbroszczyk[140], M. Zhalov[89], H. Zhang[7,21], X. Zhang[7,75], Y. Zhang[7], C. Zhang[53], Z. Zhang[7], C. Zhao[20], N. Zhigareva[54], D. Zhou[7], Y. Zhou[84], Z. Zhou[21], H. Zhu[7,21], J. Zhu[7,116], X. Zhu[7], A. Zichichi[12,26], A. Zimmermann[96], M. B. Zimmermann[34,61], S. Zimmermann[115], G. Zinovjev[3], J. Zmeskal[115]

[1] A.I. Alikhanyan National Science Laboratory (Yerevan Physics Institute) Foundation, Yerevan, Armenia
[2] Benemérita Universidad Autónoma de Puebla, Puebla, Mexico
[3] Bogolyubov Institute for Theoretical Physics, Kiev, Ukraine
[4] Department of Physics and Centre for Astroparticle Physics and Space Science (CAPSS), Bose Institute, Kolkata, India

[5] Budker Institute for Nuclear Physics, Novosibirsk, Russia
[6] California Polytechnic State University, San Luis Obispo, CA, USA
[7] Central China Normal University, Wuhan, China
[8] Centre de Calcul de l'IN2P3, Villeurbanne, Lyon, France
[9] Centro de Aplicaciones Tecnológicas y Desarrollo Nuclear (CEADEN), Havana, Cuba
[10] Centro de Investigaciones Energéticas Medioambientales y Tecnológicas (CIEMAT), Madrid, Spain
[11] Centro de Investigación y de Estudios Avanzados (CINVESTAV), Mexico City, Mérida, Mexico
[12] Centro Fermi-Museo Storico della Fisica e Centro Studi e Ricerche "Enrico Fermi', Rome, Italy
[13] Chicago State University, Chicago, IL, USA
[14] China Institute of Atomic Energy, Beijing, China
[15] COMSATS Institute of Information Technology (CIIT), Islamabad, Pakistan
[16] Departamento de Física de Partículas and IGFAE, Universidad de Santiago de Compostela, Santiago de Compostela, Spain
[17] Department of Physics, Aligarh Muslim University, Aligarh, India
[18] Department of Physics, Ohio State University, Columbus, OH, USA
[19] Department of Physics, Sejong University, Seoul, South Korea
[20] Department of Physics, University of Oslo, Oslo, Norway
[21] Department of Physics and Technology, University of Bergen, Bergen, Norway
[22] Dipartimento di Fisica dell'Università 'La Sapienza' and Sezione INFN, Rome, Italy
[23] Dipartimento di Fisica dell'Università and Sezione INFN, Cagliari, Italy
[24] Dipartimento di Fisica dell'Università and Sezione INFN, Trieste, Italy
[25] Dipartimento di Fisica dell'Università and Sezione INFN, Turin, Italy
[26] Dipartimento di Fisica e Astronomia dell'Università and Sezione INFN, Bologna, Italy
[27] Dipartimento di Fisica e Astronomia dell'Università and Sezione INFN, Catania, Italy
[28] Dipartimento di Fisica e Astronomia dell'Università and Sezione INFN, Padua, Italy
[29] Dipartimento di Fisica 'E.R. Caianiello' dell'Università and Gruppo Collegato INFN, Salerno, Italy
[30] Dipartimento DISAT del Politecnico and Sezione INFN, Turin, Italy
[31] Dipartimento di Scienze e Innovazione Tecnologica dell'Università del Piemonte Orientale and INFN Sezione di Torino, Alessandria, Italy
[32] Dipartimento Interateneo di Fisica 'M. Merlin' and Sezione INFN, Bari, Italy
[33] Division of Experimental High Energy Physics, University of Lund, Lund, Sweden
[34] European Organization for Nuclear Research (CERN), Geneva, Switzerland
[35] Excellence Cluster Universe, Technische Universität München, Munich, Germany
[36] Faculty of Engineering, Bergen University College, Bergen, Norway
[37] Faculty of Mathematics, Physics and Informatics, Comenius University, Bratislava, Slovakia
[38] Faculty of Nuclear Sciences and Physical Engineering, Czech Technical University in Prague, Prague, Czech Republic
[39] Faculty of Science, P.J. Šafárik University, Košice, Slovakia
[40] Faculty of Technology, Buskerud and Vestfold University College, Tonsberg, Norway
[41] Frankfurt Institute for Advanced Studies, Johann Wolfgang Goethe-Universität Frankfurt, Frankfurt, Germany
[42] Gangneung-Wonju National University, Gangneung, South Korea
[43] Department of Physics, Gauhati University, Guwahati, India
[44] Helmholtz-Institut für Strahlen- und Kernphysik, Rheinische Friedrich-Wilhelms-Universität Bonn, Bonn, Germany
[45] Helsinki Institute of Physics (HIP), Helsinki, Finland
[46] Hiroshima University, Hiroshima, Japan
[47] Indian Institute of Technology Bombay (IIT), Mumbai, India
[48] Indian Institute of Technology Indore, Indore, India
[49] Indonesian Institute of Sciences, Jakarta, Indonesia
[50] Inha University, Incheon, South Korea
[51] Institut de Physique Nucléaire d'Orsay (IPNO), Université Paris-Sud, CNRS-IN2P3, Orsay, France
[52] Institute for Nuclear Research, Academy of Sciences, Moscow, Russia
[53] Institute for Subatomic Physics of Utrecht University, Utrecht, Netherlands
[54] Institute for Theoretical and Experimental Physics, Moscow, Russia
[55] Institute of Experimental Physics, Slovak Academy of Sciences, Košice, Slovakia

[56] Institute of Physics, Academy of Sciences of the Czech Republic, Prague, Czech Republic
[57] Institute of Physics, Bhubaneswar, India
[58] Institute of Space Science (ISS), Bucharest, Romania
[59] Institut für Informatik, Johann Wolfgang Goethe-Universität Frankfurt, Frankfurt, Germany
[60] Institut für Kernphysik, Johann Wolfgang Goethe-Universität Frankfurt, Frankfurt, Germany
[61] Institut für Kernphysik, Westfälische Wilhelms-Universität Münster, Münster, Germany
[62] Instituto de Ciencias Nucleares, Universidad Nacional Autónoma de México, Mexico City, Mexico
[63] Instituto de Física, Universidade Federal do Rio Grande do Sul (UFRGS), Porto Alegre, Brazil
[64] Instituto de Física, Universidad Nacional Autónoma de México, Mexico City, Mexico
[65] IRFU, CEA, Université Paris-Saclay, F-91191 Gif-sur-Yvette France, Saclay, France
[66] iThemba LABS, National Research Foundation, Somerset West, South Africa
[67] Joint Institute for Nuclear Research (JINR), Dubna, Russia
[68] Konkuk University, Seoul, South Korea
[69] Korea Institute of Science and Technology Information, Daejeon, South Korea
[70] KTO Karatay University, Konya, Turkey
[71] Laboratoire de Physique Corpusculaire (LPC), Clermont Université, Université Blaise Pascal, CNRS-IN2P3, Clermont-Ferrand, France
[72] Laboratoire de Physique Subatomique et de Cosmologie, Université Grenoble-Alpes, CNRS-IN2P3, Grenoble, France
[73] Laboratori Nazionali di Frascati, INFN, Frascati, Italy
[74] Laboratori Nazionali di Legnaro, INFN, Legnaro, Italy
[75] Lawrence Berkeley National Laboratory, Berkeley, CA, USA
[76] Moscow Engineering Physics Institute, Moscow, Russia
[77] Nagasaki Institute of Applied Science, Nagasaki, Japan
[78] Physics Department, National and Kapodistrian University of Athens, Athens, Greece
[79] National Centre for Nuclear Studies, Warsaw, Poland
[80] National Institute for Physics and Nuclear Engineering, Bucharest, Romania
[81] National Institute of Science Education and Research, Bhubaneswar, India
[82] National Nuclear Research Center, Baku, Azerbaijan
[83] National Research Centre Kurchatov Institute, Moscow, Russia
[84] Niels Bohr Institute, University of Copenhagen, Copenhagen, Denmark
[85] Nikhef, Nationaal instituut voor subatomaire fysica, Amsterdam, Netherlands
[86] Nuclear Physics Group, STFC Daresbury Laboratory, Daresbury, UK
[87] Nuclear Physics Institute, Academy of Sciences of the Czech Republic, Řež u Prahy, Czech Republic
[88] Oak Ridge National Laboratory, Oak Ridge, TN, USA
[89] Petersburg Nuclear Physics Institute, Gatchina, Russia
[90] Physics Department, Creighton University, Omaha, NE, USA
[91] Physics Department, Panjab University, Chandigarh, India
[92] Physics Department, University of Cape Town, Cape Town, South Africa
[93] Physics Department, University of Jammu, Jammu, India
[94] Physics Department, University of Rajasthan, Jaipur, India
[95] Physikalisches Institut, Eberhard Karls Universit?t Tübingen, Tübingen, Germany
[96] Physikalisches Institut, Ruprecht-Karls-Universität Heidelberg, Heidelberg, Germany
[97] Physik Department, Technische Universität München, Munich, Germany
[98] Purdue University, West Lafayette, IN, USA
[99] Pusan National University, Pusan, South Korea
[100] Research Division and ExtreMe Matter Institute EMMI, GSI Helmholtzzentrum für Schwerionenforschung GmbH, Darmstadt, Germany
[101] Rudjer Bošković Institute, Zagreb, Croatia
[102] Russian Federal Nuclear Center (VNIIEF), Sarov, Russia
[103] Saha Institute of Nuclear Physics, Kolkata, India
[104] School of Physics and Astronomy, University of Birmingham, Birmingham, UK
[105] Sección Física, Departamento de Ciencias, Pontificia Universidad Católica del Perú, Lima, Peru
[106] Sezione INFN, Bari, Italy

[107] Sezione INFN, Bologna, Italy
[108] Sezione INFN, Cagliari, Italy
[109] Sezione INFN, Catania, Italy
[110] Sezione INFN, Padua, Italy
[111] Sezione INFN, Rome, Italy
[112] Sezione INFN, Trieste, Italy
[113] Sezione INFN, Turin, Italy
[114] SSC IHEP of NRC Kurchatov institute, Protvino, Russia
[115] Stefan Meyer Institut für Subatomare Physik (SMI), Vienna, Austria
[116] SUBATECH, Ecole des Mines de Nantes, Université de Nantes, CNRS-IN2P3, Nantes, France
[117] Suranaree University of Technology, Nakhon Ratchasima, Thailand
[118] Technical University of Košice, Košice, Slovakia
[119] Technical University of Split FESB, Split, Croatia
[120] The Henryk Niewodniczanski Institute of Nuclear Physics, Polish Academy of Sciences, Kraków, Poland
[121] Physics Department, The University of Texas at Austin, Austin, TX, USA
[122] Universidad Autónoma de Sinaloa, Culiacán, Mexico
[123] Universidade de São Paulo (USP), São Paulo, Brazil
[124] Universidade Estadual de Campinas (UNICAMP), Campinas, Brazil
[125] Universidade Federal do ABC, Santo Andre, Brazil
[126] University of Houston, Houston, TX, USA
[127] University of Jyväskylä, Jyväskylä, Finland
[128] University of Liverpool, Liverpool, UK
[129] University of Tennessee, Knoxville, TN, USA
[130] University of the Witwatersrand, Johannesburg, South Africa
[131] University of Tokyo, Tokyo, Japan
[132] University of Tsukuba, Tsukuba, Japan
[133] University of Zagreb, Zagreb, Croatia
[134] Université de Lyon, Université Lyon 1, CNRS/IN2P3, IPN-Lyon, Villeurbanne, Lyon, France
[135] Université de Strasbourg, CNRS, IPHC UMR 7178, 67000 Strasbourg, France
[136] Università degli Studi di Pavia, Pavia, Italy
[137] Università di Brescia, Brescia, Italy
[138] V. Fock Institute for Physics, St. Petersburg State University, St. Petersburg, Russia
[139] Variable Energy Cyclotron Centre, Kolkata, India
[140] Warsaw University of Technology, Warsaw, Poland
[141] Wayne State University, Detroit, MI, USA
[142] Wigner Research Centre for Physics, Hungarian Academy of Sciences, Budapest, Hungary
[143] Yale University, New Haven, CT, USA
[144] Yonsei University, Seoul, South Korea
[145] Zentrum für Technologietransfer und Telekommunikation (ZTT), Fachhochschule Worms, Worms, Germany

[a] Deceased
[b] Also at: Georgia State University, Atlanta, Georgia, United States
[c] Also at: Also at Department of Applied Physics, Aligarh Muslim University, Aligarh, India
[d] Also at: M.V. Lomonosov Moscow State University, D.V. Skobeltsyn Institute of Nuclear, Physics, Moscow, Russia